Information Sciences 179 (2009) 3998–4028

Contents lists available at ScienceDirect

Information Sciences

journal homepage: www.elsevier.com/locate/ins

An experimental study on the applicability of evolutionary algorithms to craniofacial superimposition in forensic identification

Oscar Ibáñez [a,*], Lucia Ballerini [b], Oscar Cordón [a], Sergio Damas [a], José Santamaría [c]

[a] European Centre for Soft Computing, Mieres, Asturias, Spain
[b] Institute of Perception, Action and Behaviour, University of Edinburgh, Edinburgh, UK
[c] Dpt. Computer Science, University of Jaén, Jaén, Spain

ARTICLE INFO

Article history:
Received 13 March 2008
Received in revised form 16 October 2008
Accepted 25 December 2008

Keywords:
Forensic identification
Craniofacial superimposition
Image registration
Evolutionary algorithms
Real-coded genetic algorithms
CMA-ES

ABSTRACT

Photographic supra-projection is a forensic process that aims to identify a missing person from a photograph and a skull found. One of the crucial tasks throughout all this process is the craniofacial superimposition which tries to find a good fit between a 3D model of the skull and the 2D photo of the face. This photographic supra-projection stage is usually carried out manually by forensic anthropologists. It is thus very time consuming and presents several difficulties. In this paper, we aim to demonstrate that real-coded evolutionary algorithms are suitable approaches to tackle craniofacial superimposition. To do so, we first formulate this complex task in forensic identification as a numerical optimization problem. Then, we adapt three different evolutionary algorithms to solve it: two variants of a real-coded genetic algorithm and the state of the art evolution strategy CMA-ES. We also consider an existing binary-coded genetic algorithm as a baseline. Results on several superimposition problems of real-world identification cases solved by the Physical Anthropology lab at the University of Granada (Spain) are considered to test our proposals.

1. Introduction

Forensic anthropology is best conceptualized more broadly as a field of forensic assessment of human skeletonized remains and their environments [32]. This assessment includes both the identification of the victims' physical characteristics and cause and manner of death from the skeleton. This way, the most important application of forensic anthropology is the identification of human beings from their skeletal remains.

Photographic supra-projection [30] is a forensic process where photographs or video shots of a missing person are compared with the skull that is found. By projecting both photographs on top of each other (or, even better, matching a scanned three-dimensional skull model against the face photo/video shot), the forensic anthropologist can try to establish whether that is the same person.

To do so, an accurate 3D model of the skull is first demanded. The forensic experts select some facial anthropometric landmarks in the subject photograph, and cranial anthropometric landmarks in the obtained skull model. Next, the matching of these two sets of radiometric points is considered to guide the superimposition of the skull 3D model and the photograph, through a process known as craniofacial superimposition [30]. Then, a decision making stage starts by analyzing the different kinds of achieved matchings between landmarks. Some of them will perfectly match, some will partially do so and finally some others will not. After the whole process, the forensic expert must declare whether the analyzed skull corresponds to the missing person or not.

* Corresponding author. Tel.: +34 985 456545; fax: +34 985 456699.
E-mail address: oscar.ibanez@softcomputing.es (O. Ibáñez).

0020-0255/$ - see front matter © 2009 Elsevier Inc. All rights reserved.
doi:10.1016/j.ins.2008.12.029

The craniofacial superimposition process is known to be one of the most time consuming tasks for the forensic experts. In addition, there is not a systematic methodology but every expert usually applies a particular process. Hence, there is a strong interest in designing automatic methods to support the forensic anthropologist to put it into effect [46].

On the other hand, image registration (IR) [54] is a fundamental task in image analysis. It aims to find a correspondence (or transformation) among two or more images taken under different conditions, i.e. at different times, from different viewpoints, using different sensors, or a combination of them. Thus, the key idea of the IR process is achieving the transformation (rotation, translation, etc.) that places different images in a common coordinate system bringing the points as close together as possible. This is done by an optimization process which aims to minimize the error of a given metric of resemblance. Evolutionary algorithms (EAs) [5,6,19] in general, and genetic algorithms (GAs) [23,33] in particular, have been successfully applied to tackle different IR problems [16,38,43,50].

A sensible way to design an automatic craniofacial superimposition procedure is through the use of a IR technique to properly align the 3D model and the 2D image in a common coordinate frame. Unfortunately, we can only find one proposal [34] to automate the process and, as we will see in Section 5, the results achieved are not suitable for the forensic experts. From our previous experience on applying EAs to medical IR [14,15] we will formulate craniofacial superimposition as an IR problem. Then we will design different real-coded EAs to tackle this problem, comparing their performance with Nickerson et al.'s binary-coded GA [34], which shows several flaws making it unsuitable for the problem solving. We aim to automate and drastically reduce the time of the superimposition task by means of a systematic method based on EAs. Besides, this proposal can also help forensic experts as a way to obtain an initial automatic superimposition to be manually refined in a second stage, with the consequent saving of time.

The structure of this paper is as follows. In Section 2, we introduce some IR basics and briefly review the state of the art on craniofacial superimposition. In Section 3, the proposed problem formulation is detailed. Section 4 is devoted to describe the designed EAs and to explain their adaption for solving the superimposition problem. In Section 5, we will show the results on real-world cases' experiments, together with an analysis of the performance of the algorithms depending on the parameter values selected. Section 6 collects some conclusions and future works. Finally, Appendix A provides the whole experimental results obtained for the cases studied in Section 5.

2. Preliminaries

The craniofacial superimposition task is so complicated that it worths addressing some important concepts before tackling the problem itself. First we want to clarify the context of this contribution. This work is part of a project that aims to propose an automatic methodology to develop the whole photographic supra-projection process. This process is divided in three stages, somehow reproducing the steps of the procedure employed by forensic experts. The first stage involves achieving the "virtual model" of the physical object (the skull) itself, so that it constitutes an accurate model of the real object we are trying to represent, i.e., a skull model. To do so, we have successfully considered EAs as robust optimizers able to overcome the lack of experience of the forensic anthropologists on the use of the 3D scanners and the high complexity of the problem in real scenarios [39–41].

Likewise, the second step known as craniofacial superimposition aims to properly superimpose the skull 3D model and the photograph. Forensic experts extract different landmarks from the obtained skull model and from the face photograph. In our approach, these two sets of landmarks will guide the automatic search for the registration transformation parameters that accurately overlay them. In this case, that transformation corresponds to a 3D/2D one. Again, we consider EAs as a powerful tool to perform this task (as was shown in some preliminary work developed in [7]). The goal of this contribution is to formulate the corresponding IR problem and to properly solve it by means of real-coded EAs.

Finally, the last stage of the photographic supra-projection technique corresponds to the decision making. Typically, once the best superimposition is achieved, the forensic experts analyze the final correspondence between the significant landmarks of the skull and the face, and make a decision on five possible choices: positive, negative, likely positive, likely negative, or unknown identification. We aim to tackle this last procedure in the short future by means of fuzzy logic techniques reflecting the partial matching nature of the problem.

Since the first and the second photographic supra-projection stages are based on IR techniques, Section 2.1 is devoted to briefly describe the IR problem. Then, in Section 2.2 we review the state of the art on craniofacial superimposition which is the stage this paper is focused on.

2.1. The image registration problem

The key idea of the IR process is to achieve the transformation that places different 2D/3D images in a common coordinate system. There is not a universal design for a hypothetical IR method that could be applicable to all registration tasks, because various considerations of the particular application must be taken into account. Nevertheless, IR methods usually require the four following components:

– Two input 2D or 3D **Images** often named as Scene $I_s = \{\vec{p}_1, \vec{p}_2, \ldots, \vec{p}_n\}$ and Model $I_m = \{\vec{p}'_1, \vec{p}'_2, \ldots, \vec{p}'_m\}$, with $\vec{p}_i$ and $\vec{p}'_j$ being image points.

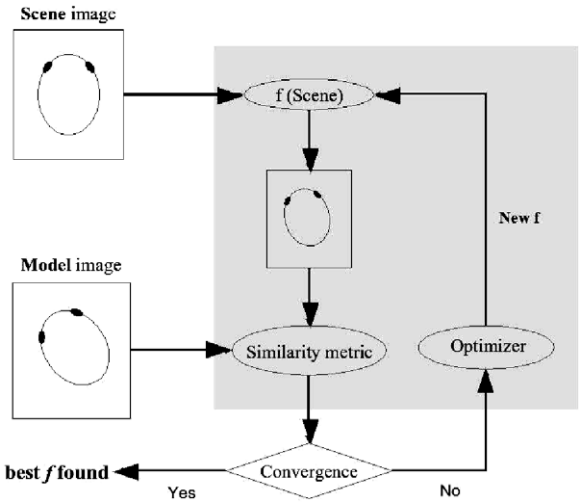

Fig. 1. The IR optimization process.

- A **Registration transformation** *f*, being a parametric function relating both images.
- A **Similarity metric function** *F*, in order to measure a qualitative value of closeness or degree of fitting between the scene and the model images.
- An **Optimizer** which looks for the optimal transformation *f* within the defined solution search space.

Hence, IR is the process of finding the optimal spatial transformation *f* achieving the best fitting (measured using *F*) between the model and the transformed scene image points, $f(I_s)$. Such transformation estimation is interpreted into an iterative optimization process in order to properly explore the search space. Fig. 1 graphically represents the IR optimization scheme.

One of the most important components of any IR method is the similarity metric. This is considered as a function *F* that measures the goodness of a given registration solution (that is, the registration transformation *f*), and the final performance of any IR method will depend on its accurate estimation.

Each solution is evaluated by *F* applying its corresponding transformation *f* to one of the two images, usually to the scene image ($f(I_s)$). There are many approaches trying to define *F* depending on the dimensionality (2D or 3D) and the nature of the considered images. When following a feature-based IR approach, i.e. when the problem is guided by a set of features selected from both the scene and the model images, the usual similarity metric is the Mean Square Error (MSE) [9,40,50,52]:

$$F(I_s, I_m, f) = \frac{1}{r}\sum_{i=1}^{r} \|f(\vec{p}_i) - \vec{p}'_j\|^2 \tag{1}$$

where *r* is the number of points in the scene image, $f(\vec{p}_i)$ is the resulting point after the transformation is applied to the scene point $\vec{p}_i$, $\vec{p}'_j$ is the closest model point to $f(\vec{p}_i)$ of the scene, and $\|\cdot\|$ is the 2D Euclidean distance.

2.2. State of the art on craniofacial superimposition

Successful comparison of human skeleton remains with artistic or photographic replicas has been achieved many times, ranging from the studies of the skeletal remains of Dante in the nineteenth century [49] to the identification of victims of the recent Indian Ocean tsunami [2]. Craniofacial identification is thus a challenging problem in forensic anthropology that has been tackled since long time ago [30] to put the photographic supra-projection process into effect. Nevertheless, to date, no automatic method is used in practical applications despite the high number of cases examined [46].

Recent papers confirm that some authors think the most advanced method is based on digital superimposition through the use of Adobe Photoshop® and Corel Draw® and the imaging tools provided by these software packages [2,10,37]. We agree with these authors that working with digital images is definitively simpler and cheaper than with photographic or video superimposition equipments. However, we should note that the methods they use are not automatic as they manually resize, shift and rotate the images by trial and error, thus dealing with a very time consuming and error affected process. It is worth mentioning that the forensic expert may even employ up to 24 h for each case, working in the latter way.

All the researchers agree that a key problem of photographic supra-projection is the size and orientation of the skull to correctly match the head in the photo. Different methods for the craniofacial superimposition stage have been proposed. Some of these approaches were classified in a review by Aulsebrook et al. [4] according to the technology they used, i.e. static photographic transparency, video technology, and computer graphics. In a previous paper [8], we proposed a new taxonomy

for photographic supra-projection methods considering an up-to-date classification criterion, more related to the use of computers, and differentiating between automatic and not automatic methods.

Indeed, the differentiation between methods that do not use computer technology and methods that actually use it had already been proposed. In the literature, photographic and video superimposition have been considered to belong to the first category. Meanwhile, methods defined as digital or computer-aided superimposition had been included in the second one. We expanded the latter class by differentiating between computer-assisted and computer-based methods. The former ones use computers to support the superimposition process and/or to visualize the skull and the face. Nevertheless, the size and orientation of the skull is changed manually to correctly match the pose of the head in the photograph. This is achieved by either physically moving the skull, where computers are simply used to visualize it on the monitor, or by manually moving its digital image on the screen (with the help of some commercial software) until a good match is found. The works of Ricci et al. [36], Ubelaker et al. [47] and Yoshino et al. [51], are typical examples of what we call computer-assisted superimposition in the sense that a digital infrastructure supports the process, but its potential utility is not used to automate it.

The latter ones, i.e. computer-based craniofacial superimposition methods, automatically find the optimal superimposition between the 3D skull and the 2D face photograph using computer algorithms. Up to our knowledge, there are only two proposals performing craniofacial superimposition in a fully automatic way, based on the use of neural networks [22] and GAs [34], respectively. However, as we will see in the following, they are not suitable for forensic experts.

The method proposed by Ghosh and Sinha [22] was an adaptation of their previous proposal for face recognition problems [44]. The Extended Symmetry Perceiving Adaptive Neuronet (ESPAN) consisted of two neural networks to be applied to two different parts of the overlaying and allows the user to select fuzzy facial features to account for ambiguities due to soft tissue thickness. More in details, the system was able to implement an objective assessment of the symmetry between two nearly front images, the cranial image and the facial image, which were the inputs as the source and the target images, respectively. The output was the mapped cranial image suitable for superimposition. Two networks needed to be trained separately because each of them was able to correctly map only a part of the cranial image. Two limitations, already pointed out by the authors, were the existence of a part of the cranial image that would never be properly mapped and the need of a frontal view image. In addition, the method is only valid for 2D images, i.e., it is not able to handle a 3D skull model but just a less informative 2D skull photograph. Finally it was not fully applicable because of its long computation time and the need of separately applying two different networks to the upper skull contour and to frontal view cranial features. The overlaying found by the first one could be disrupted by the second.

Nickerson et al.'s method [34] used a binary-coded GA (BCGA) to find the optimal parameters of the similarity and perspective transformation that overlays the 3D skull model on the face photograph. More in details, this method included the following tasks:

- 2D digitalization of an antemortem facial photograph.
- 3D digitalization of the surface mesh of the skull.
- Application of digital filtering techniques to the 2D photo image and the 3D model to reduce or eliminate systematic error.
- Selection of four landmark points on the digital facial image and four equivalent non-coplanar landmarks on the skull surface mesh.
- Calculation of the near-optimal affine and perspective transformations required to map the skull surface mesh into two dimensions and onto the face image.
- Joint solid rendering of the digital facial photograph and transformed skull surface mesh for visual analysis.

Fig. 2. Cranial and facial landmarks.

A digital camera and a laser range scanner were used for 2D and 3D digitalizations, respectively. Well known image processing algorithms were considered for image enhancement. Rendering was done through computer graphics techniques, after polygonal texture mapping of the 2D image.

The most important novelty of this technique was the automatic calculation of the mapping of the skull surface mesh on the digital facial photograph. This mapping was achieved from the matching of the four landmarks previously identified both in the face and the skull. The landmarks they used: either the *glabella* or the *nasion*, the two *ectocanthion* points, and an upper mandibular dentition point, if present, or the *subnasal* point (see Fig. 2).

Three approaches were considered to solve the optimization problem: a heuristic technique, a classic numerical optimization method, and a BCGA. Results based on the GA outperformed the remainder.

According to Ghosh et al. [22], Nickerson et al.'s method did not gain much popularity due to the fact that it essentially required a digitalized 3D cranial image reconstruction, which could not be implemented either by an easy/simple procedure or by an economic hardware configuration. We think the reason for not finding practical applications of this method is probably also due to the lack of important design issues in the description of the method. Besides, it could have been difficult for forensic experts to understand the mathematical formulation of the registration problem and the evolutionary framework (especially considering there are important issues missing). Finally, the most important drawback of this technique is its lack of accuracy when dealing with real-world identification cases, as we will see in Section 5.

On the other hand, we should mention that several automatic approaches regarding the 3D face model–2D face photograph superimposition have also been presented [13,24] and extensive reviews can be found like the one in Ref. [12]. However, they are out of the scope of this discussion, as they deal with face recognition that is a completely different problem involving the superimposition of a 3D image of an object (the face 3D model) with a 2D projection of the same object (the face 2D photograph). Notice that, craniofacial superimposition is an even more challenging problem where the two objects to be matched are different (a skull 3D model and a face 2D photo). In face recognition, there is no need to tackle with the uncertainty involved in real cases of craniofacial superimposition, where the thickness of the soft tissue has to be taken in account. Moreover, in the former scenarios, all the data relative to the camera are known. These data are not always available in real-world forensic identification cases. The photographs are provided by the relatives without any additional information and, in some cases, they are also modified by preprocessing algorithms (size cropping and rescaling, color and contrast transformation, etc.) which may negatively influence the results of the superimposition.

3. Problem description

In Section 2, we presented the similarities between craniofacial superimposition and the IR problem. This section aims to supply an insight into such relationship describing the geometric transformation involved in craniofacial superimposition in order to be able to provide the formal problem statement.

3.1. Introduction

The final goal of the IR problem associated to craniofacial superimposition is to find a transformation that, when applied to the skull, can locate it exactly in the same pose it had when the available photograph of the missing person was taken. Along this process, we can easily differentiate two important moments (Fig. 3). First, when the missing person was posing for the photograph. Second, when the skull found was scanned to obtain a skull 3D model that could be geometrically transformed in order to achieve the desired location. Hence, it is a really complex problem because we are trying to reproduce the scenario when the subject photograph was taken with an important number of unknowns coming from two different sources:

Fig. 3. Photograph and skull model acquisitions.

- The camera configuration. At the moment of the acquisition, there were different parameters that have an influence in the craniofacial superimposition problem. Some of them are directly reflected on the photograph as the specific area of interest for the person taking it (highlighted in the example shown in the left side of Fig. 3 using a dashed rectangle) or the lighting conditions. However, there are some other parameters that cannot be easily derived from the photograph as the distance from the camera to the missing person or the aperture of the camera that will determine what is finally projected into the photograph and what is outside it. Indeed, if a camera with a wide-angle lens was used it would be possible to acquire a wider piece of the scene while keeping the same distance to the object one wanted to photograph.
- The skull model. Once the first stage of the photographic supra-projection process is finished, a skull 3D model is available. This skull model will have a specific orientation, resolution and size given by the technical features of the scanner as well as by the skull modeling process (Fig. 3, right). Notice that the skull model size usually corresponds to the size of the real skull.

3.2. Geometric transformations for the IR problem underlying craniofacial superimposition

This section aims to present the geometric transformations involved in the craniofacial superimposition problem. A detailed description of projective geometry is out of the scope of this contribution, the interested reader is referred to Ref. [21]. The set of geometric transformations needed to accomplish the superimposition task follows:

- **Rotation *R***: The first step to find the proper location of the skull will involve applying a rotation to orient the skull in the same pose of the photograph. In order to define a rotation, the direction of the rotation axis $\vec{d} = (d_x, d_y, d_z)$, the location of the rotation axis with respect to the center of coordinates $\vec{r} = (r_x, r_y, r_z)$, and the angle θ must be given. Once they are determined, the usual computer graphics procedure to apply this rotation is as follows:
  - Translate the skull to align the origin of coordinates with the rotation axis.
  - Rotate the skull so that the rotation axis coincides with one of the Cartesian axes.
  - Perform the rotation given by θ.
  - Use the inverse rotation matrices in reverse order in order to leave the rotation axis in its original orientation.
  - Apply the inverse translation matrix to leave the rotated skull in its original location.

  This rotation process R is thus given by:

$$R = (A \cdot D_1 \cdot D_2 \cdot \Theta \cdot D_2^{-1} \cdot D_1^{-1} \cdot A^{-1}) \tag{2}$$

  where

$$A = \begin{bmatrix} 1 & 0 & 0 & 0 \\ 0 & 1 & 0 & 0 \\ 0 & 0 & 1 & 0 \\ -r_x & -r_y & -r_z & 1 \end{bmatrix}, \quad D_1 = \begin{bmatrix} 1 & 0 & 0 & 0 \\ 0 & d_z/v & d_y/v & 0 \\ 0 & -d_y/v & d_z/v & 0 \\ 0 & 0 & 0 & 1 \end{bmatrix}, \quad D_2 = \begin{bmatrix} v & 0 & d_x & 0 \\ 0 & 1 & 0 & 0 \\ -d_x & 0 & v & 0 \\ 0 & 0 & 0 & 1 \end{bmatrix},$$

$$\Theta = \begin{bmatrix} \cos\Theta & -\sin\Theta & 0 & 0 \\ \sin\Theta & \cos\Theta & 0 & 0 \\ 0 & 0 & 1 & 0 \\ 0 & 0 & 0 & 1 \end{bmatrix}, \quad v = \sqrt{d_y^2 + d_z^2}$$

- **Scaling** S: The size of the skull model must be uniformly adapted according to the size of the missing person in the photograph. Hence, the coordinates of each point of the skull model will be resized considering a factor named s:

$$S = \begin{bmatrix} s & 0 & 0 & 0 \\ 0 & s & 0 & 0 \\ 0 & 0 & s & 0 \\ 0 & 0 & 0 & 1 \end{bmatrix}$$

- **Translation** T: The coordinates of the skull model are relative to the origin defined by the range scanner. Thus, it must be translated according to $T = (t_x, t_y, t_z)$ in order to be located in front of the camera and reproduce the conditions when the photograph of the missing person was taken. To do so, the following matrix is considered:

$$T = \begin{bmatrix} 1 & 0 & 0 & 0 \\ 0 & 1 & 0 & 0 \\ 0 & 0 & 1 & 0 \\ t_x & t_y & t_z & 1 \end{bmatrix}$$

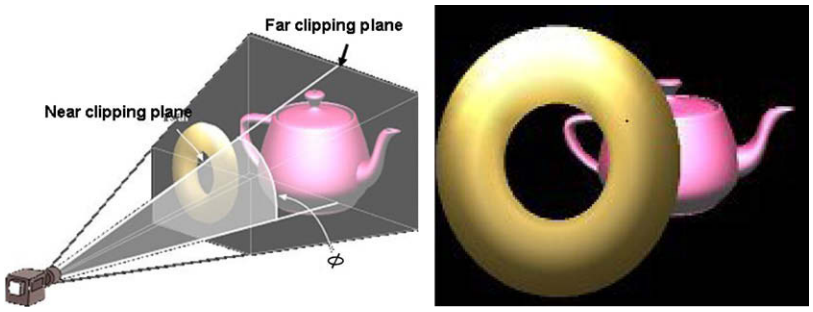

Fig. 4. Camera configuration with angle of view ϕ (left) and the corresponding photograph (right).

– **Perspective projection** P: Cameras perform a perspective projection of the scene into the photograph in order to provide a more realistic perception of how far the object is from the viewer. In computer graphics, this effect is achieved defining a frustum[1] of a rectangular pyramid (Fig. 4, left). There are thus two planes that are used to delimit what is visible in the scene and what is consequently represented in the computer. Those parts of the scene that are closer to the camera than the near clipping plane (NCP) or farther than the far clipping plane (FCP) will not be considered for visualization purposes. They will be outside the field of view of the camera. This issue has also a direct effect on the geometric transformation of the skull we are describing.
Once the previous transformations are applied, the skull is located in front of the camera, with the proper orientation and size. Finally, we need to determine how far the camera is from the skull. If it is too close then the camera will capture just a projection of the skull without the rest of the elements that were captured in the photograph. This issue has a strong connection to the angle of view (ϕ) of the camera, which describes the angular extent of a given scene that is imaged by a camera. Fig. 4 depicts this effect. Notice that, although the torus has a smaller size than the teapot in the real world (Fig. 4, left), the former seems to be bigger than the latter in the picture acquired by the camera (Fig. 4, right) because of the effect of the perspective when the object is too close to the camera. Once the camera is located in the proper position, all the rays connecting every 3D landmark of the skull with its corresponding 2D landmark in the photograph will converge in the center of projection. In addition, we should note that the torus is fully visible in the picture that has been acquired (Fig. 4, right). However, if it had been placed slightly on the left then it would have been partially outside the defined frustum and there would be part of it missing in the picture.The perspective transformation described is given by:

$$P = \begin{bmatrix} 1 & 0 & 0 & 0 \\ 0 & 1 & 0 & 0 \\ 0 & 0 & \tan(\phi/2) & \tan(\phi/2) \\ 0 & 0 & 0 & 1 \end{bmatrix}$$

3.3. Problem statement

Given two sets of 2D facial and 3D cranial landmarks (F and C, respectively):

$$F = \begin{bmatrix} x_{f_1} & y_{f_1} & 1 & 1 \\ x_{f_2} & y_{f_2} & 1 & 1 \\ \vdots & \vdots & \vdots & \vdots \\ x_{f_N} & y_{f_N} & 1 & 1 \end{bmatrix}, \quad C = \begin{bmatrix} x_{c_1} & y_{c_1} & z_{c_1} & 1 \\ x_{c_2} & y_{c_2} & z_{c_2} & 1 \\ \vdots & \vdots & \vdots & \vdots \\ x_{c_N} & y_{c_N} & z_{c_N} & 1 \end{bmatrix}$$

we aim to solve the following system of equations with twelve unknowns $(r_x, r_y, r_z, d_x, d_y, d_z, \theta, s, t_x, t_y, t_z, \phi)$ that represents the geometric transformation which maps every cranial landmark C_i in the skull 3D model onto its corresponding facial landmark F_i in the photograph:

$$F = C \cdot (A \cdot D_1 \cdot D_2 \cdot \theta \cdot D_2^{-1} \cdot D_1^{-1} \cdot A^{-1}) \cdot S \cdot T \cdot P \tag{3}$$

4. Design of real-coded evolutionary algorithms for craniofacial superimposition

EAs have been successfully applied to a variety of IR problems [16]. As we explained in Section 3, craniofacial superimposition can be formulated as a numerical optimization problem with twelve unknowns in the framework of IR. Next, we

[1] A frustum is the portion of a solid – normally a cone or a pyramid – which lies between two parallel planes cutting the solid.

propose four different EA designs in order to deal with this complex IR problem. Before going through them, we will firstly describe the common components to solve the superimposition problem.

4.1. Common components to solve the craniofacial superimposition problem by means of real-coded evolutionary algorithms

In Section 3 we described the geometric transformation f for the IR problem underlying craniofacial superimposition. This transformation f is determined fixing the aforementioned 12 unknowns. We consider a coding scheme representing these twelve unknowns in a vector of real numbers to be evolved by means of the real-coded EAs designed in this contribution. Hence, our individual will have the following form:

$$\boxed{r_x}\boxed{r_y}\boxed{r_z}\boxed{d_x}\boxed{d_y}\boxed{d_z}\boxed{\theta}\boxed{\mathrm{s}}\boxed{t_x}\boxed{t_y}\boxed{t_z}\boxed{\phi}$$

In order to adapt these twelve parameters through the use of evolutionary operators, their ranges must be defined. We have calculated them as follows:

$$\begin{aligned}
&r_i \in [\mathit{Centroid} - \mathit{radius}, \mathit{Centroid} + \mathit{radius}], \quad i \in \{x, y, z\}\\
&d_i \in [-1, 1], \quad i \in \{x, y, z\}\\
&\theta \in [0^\circ, 360^\circ]\\
&s \in [0.25, 2]\\
&\phi \in [10^\circ, 150^\circ]\\
&t_x \in [-\mathit{length}_{\mathrm{FB}} - (C_x + \mathit{radius}), \mathit{length}_{\mathrm{FB}} - (C_x - \mathit{radius})]\\
&t_y \in [-\mathit{length}_{\mathrm{FB}} - (C_y + \mathit{radius}), \mathit{length}_{\mathrm{FB}} - (C_y - \mathit{radius})]\\
&t_z \in [\mathrm{NCP} - (C_z + \mathit{radius}), \mathrm{FCP} - (C_z - \mathit{radius})]
\end{aligned}$$

where $\mathit{radius} = \max(\|\mathit{Centroid} - C_j\|)$, with *Centroid* being the centroid of the considered 3D landmarks, C_j being the jth 3D cranial landmark and $\|\cdot\|$ being the Euclidean distance between two 3D points; FCP and NCP are the Far and Near Clipping Planes, respectively; FB is the frustum Base; and

$$\mathit{length}_{\mathrm{FB}} = \frac{(\min_{\mathrm{FD}} + \mathrm{FCP}) * \sin\left(\frac{\phi_{\max}}{2}\right)}{\sin\left(90^\circ - \left(\frac{\phi_{\max}}{2}\right)\right)}$$

with FD being the Focal Distance and

$$\min_{\mathrm{FD}} = \frac{1}{\tan\left(\frac{\phi_{max}}{2}\right)}$$

considering a 2×2 projection plane centered in the *Z-axis* (see Section 3.2).

In preliminary experiments, we considered a higher scaling upper bound but we did not achieve better results. On the other hand, we should note that the field of view of a typical camera is $\phi = 45^\circ$. However, in professional ones, where even the lens can be changed, $\phi \in [5^\circ, 180^\circ]$.

To measure the quality of the registration transformation encoded in a specific individual a fitness function is needed. Therefore, given $C = \{C_1, C_2, \ldots, C_N\}$ and $F = \{F_1, F_2, \ldots, F_N\}$, two sets of 3D cranial and 2D facial landmarks, respectively, we propose the minimization of the following fitness function for all the evolutionary approaches to the problem being considered:

$$\mathrm{fitness} = \beta_1 \cdot \mathrm{MSE} + \hat{w} \cdot \beta_2 \cdot \mathrm{MAX} \tag{4}$$

where

$$\mathrm{MSE} = \frac{\sum_{i=1}^{N} \|f(C_i) - F_i\|^2}{N} \tag{5}$$

and

$$\mathrm{MAX} = \mathrm{MAX}_{i=1}^{N} \|f(C_i) - F_i\|^2 \tag{6}$$

with $\|\cdot\|$ being the 2D Euclidean distance, N being the number of considered landmarks and $f(C_i)$ being the positions of the transformed 3D landmarks once they have been spatially relocated and projected in the projection plane.

The scaling factor $\hat{w}$ (used when $\beta_1 \neq 0$ and $\beta_2 \neq 0$) is obtained by averaging the proportion between MSE and MAX (noted by w_{S_i}) for each individual S_i of the initial population (P_0):

$$\hat{w} = \frac{\sum_{i=1}^{M} w_{S_i}}{M} \tag{7}$$

where $w_{S_i} = \mathrm{MSE}(S_i)/\mathrm{MAX}(S_i)$ and M is the EA population size.

Finally, there is something important to take into account when trying to project 3D images in a 2D plane by means of the formulation introduced in Section 3. There are lots of values for the twelve unknowns (transformation parameters) which correspond to a non-projectable solution. This is due to the perspective projection (see Section 3.2) and, depending on the transformation parameters values, the skull projection can be outside of the 2D image area. Hence, we are dealing with a multimodal problem with restrictions and, to solve these kinds of problem with EAs, two different approaches can be followed [6,19,23,33]. On the one hand, we can restrict the search mechanism to avoid looking into the space of non-projectable solutions. On the other hand, we can penalize non-projectable solutions by means of the fitness function to avoid moving through the non-projectable search space as much as possible. Since both solution spaces (projectable and non-projectable) are quite interlaced in our craniofacial superimposition space, we decided to implement the second approach by assigning a theoretical maximum value of penalization to the fitness of the individual when the solution is a non-projectable one. Thanks to this, we allow the genetic material of these solutions to be considered for the generation of hopefully good quality projectable solutions.

4.2. Real-coded genetic algorithms

Since GAs [23,33] are maybe the most representative EAs and the only existing proposal for our problem was based on them, we decided to start tackling craniofacial superimposition by using GAs. The natural coding considered representing the 12 registration transformation parameters in a real-valued array, lead us to use a real-coded genetic algorithm (RCGA) [28]. RCGAs have become a very active area of research in the last decade achieving very good performance in many different applications and becoming a valid alternative to evolution strategies [5] and evolutionary programming [18] for numerical optimization.

Thus, we designed a RCGA with the following features:

Initial population generation, as a consequence of the aforementioned problem of the non-projectable solutions (see Section 4.1), a considerable proportion of the initial population could correspond to this kind of solutions. Due to the inability of evaluating non-projectable solutions in terms of the proposed fitness function, we must avoid a convergence to the search space regions containing these solutions. This have to be done while keeping a useful diversity. With these aims, the initial population of the considered GA is generated as follows: new individuals are randomly created until at least the half of the population phenotypes correspond to projectable solutions.

Tournament selection method [11], in which t individuals ($t = 2$ is usually a common choice) are selected at random from the population with replacement and the best of them is inserted into the new population for further genetic processing. This procedure is repeated until the mating pool is filled.

Elitism, the individual with best (lowest) fitness value is kept unchanged in the next generation population.

Random mutation operator [6], which randomly selects one of the genes of a parent and sets it equal to a uniform random number between the gene's lower and upper bounds.

Two crossover operators, thus involving two different designs of the RCGA:

(1) the **blend crossover** (BLX-α) [20] which uniformly picks new individuals with values that lie in $[x'_i, y'_i]$, an extended interval obtained from the two parents' gene values x_i and y_i for a particular variable i. The offspring O is sampled as follows:

$$o_i = x'_i + r \times (y'_i - x'_i); \quad i = 1, \ldots, 12 \tag{8}$$

where $x'_i = x_i - \alpha \times (y_i - x_i)$; $y'_i = y + \alpha \times (y_i - x_i)$; and r is a uniform random number $\in [0, 1]$, checking that x'_i and y'_i will lie between the variable's lower and upper bounds. In our case, two offsprings are generated by applying twice the operator on the two parents.

Although BLX-α was proposed more than fifteen years ago, it has become a standard in the area due to its good performance thanks to its ability to properly establish a good exploration–exploitation trade-off. In fact, Nomura and Shimohara [35] have demonstrated theoretically that BLX-α has the ability to promote diversity in the population of an EA. They state that BLX-α spreads the distribution of the chromosomes when $\alpha > (\sqrt{3} - 1)/2$ ($\simeq$0.366), and reduces it otherwise. This property was verified through simulations.

From now on we will refer to this RCGA as RCGA-BLX-α.

(2) the **simulated binary crossover** (SBX) [17] is another real-parameter recombination operator commonly used in the literature which has shown very good results. In SBX, offspring are created in proportion to the difference in parent solutions. The procedure of computing the offspring solutions $x_i^{(1,t+1)}$ and $x_i^{(2,t+1)}$ from parent solutions $x_i^{(1,t)}$ and $x_i^{(2,t)}$ is described as follows. First, a random number u between 0 and 1 is created. Thereafter, from a specified probability distribution function:

$$P(\beta) = \begin{cases} 0.5(\eta + 1)\beta^{\eta}, & \text{if } \beta \leqslant 1 \\ 0.5(\eta + 1)/\beta^{\eta+2}, & \text{otherwise} \end{cases} \tag{9}$$

defined over a non-dimensionalized parameter $\beta = \left|\left(x_i^{(2,t+1)} - x_i^{(1,t+1)}\right) \Big/ \left(x_i^{(2,t)} - x_i^{(1,t)}\right)\right|$, the ordinate β_q is found so that the area under the probability curve from 0 to β_q is equal to the chosen random number u:

$$\beta_q = \begin{cases} (2u)^{\frac{1}{\eta+1}}, & \text{if } u \leqslant 0.5 \\ (1/(2(1-u)))^{\frac{1}{\eta+1}}, & \text{otherwise} \end{cases} \tag{10}$$

In the above expressions, the distribution index η is any non-negative real number. A large value of η allows a large probability for creating near parent solutions while a small value of η allows distant points to be created as offspring solutions. After obtaining β_q from the above probability distribution, the descendent solutions are calculated as follows:

$$x_i^{(1,t+1)} = 0.5\left[(1+\beta_q)x_i^{(1,t)} + (1-\beta_q)x_i^{(2,t)}\right] \tag{11}$$

$$x_i^{(2,t+1)} = 0.5\left[(1+\beta_q)x_i^{(1,t)} + (1-\beta_q)x_i^{(2,t)}\right] \tag{12}$$

In the remainder of the paper, this RCGA will be noted RCGA-SBX.

4.3. Covariance Matrix Adaptation Evolution Strategy

As a second approach to solve the craniofacial superimposition problem, we took the Covariance Matrix Adaptation Evolution Strategy (CMA-ES) algorithm [26,27], which is considered as the state of the art in real-coded EAs. The high performance of the CMA-ES was demonstrated in the IEEE CEC'2005 Special Session on Real Parameter Optimization. For the given set of test functions [45], it had the lowest average error rate among all the participant EAs [25].

The CMA-ES is an advanced $(\mu - \lambda)$ evolution strategy [5] that updates the covariance matrix of the multivariate normal mutation distribution. New candidate solutions are sampled according to the mutation distribution and the covariance matrix describes the pairwise dependencies between the variables in it. The decision variable matrix distribution x is specified by:

- The distribution center, which is defined by a point in the search space $\overrightarrow{m}$.
- An orientation in the coordinate axis, defined by the covariance matrix C.
- A variance, defined by the parameter σ^2.

In each generation $(t+1)$ the algorithm follows the next steps:

(i) λ offsprings are independently created following a multi-variable normal distribution:

$$\overrightarrow{x}_k^{(t+1)} \sim N(\overrightarrow{m} = \langle \overrightarrow{x} \rangle_w^t, \sigma^2 C^{(g)}) \tag{13}$$

for $k = 1, \ldots, \sigma$, where $N(\overrightarrow{m}, C)$ noted a normally random vector distributed with mean $\overrightarrow{m}$ and covariance matrix C.

(ii) The λ created solutions are evaluated and sorted depending their fitness function value.

(iii) The μ best individuals are selected.

(iv) Parameters $\overrightarrow{m}\sigma$ and C are updated only considering the μ best solutions, to focus the exploitation on the regions which contain these points.

The updating process indicated in step iv is performed as follows:

$$\overrightarrow{m} = \langle \overrightarrow{x} \rangle_w^{(t+1)} = \sum_{i=1}^{\mu} \omega_i \overrightarrow{x}_{i:\lambda}^{(t+1)} \tag{14}$$

where $\omega_i \epsilon \Re \omega_i \leqslant 0$ and $\sum_{i=1}^{\mu} \omega_i = 1$.

The equations to update the rest of the parameters (size of the distribution σ and covariance matrix C) are specified in [26].

In this way, in each iteration the set of variables are adapted. The distribution center $\overrightarrow{m}$ moves to a weighted mean of the better solutions found. The covariance matrix C is adapted to the shape of the μ best solutions created. Besides, σ is adapted depending on the obtained improvement: its value grows up if the new solutions are better than the old ones and brings down otherwise. This iterative process continue until a prefixed number of evaluations is reached.

The method only needs two parameters to be specified since in [26] the authors proposed the best values for the rest. These parameters are the initial distribution center $\overrightarrow{m} = \langle \overrightarrow{x} \rangle_\omega^{(0)}$ and the mutation normal distribution variance σ (notice that, in Section 5 we have changed the notation of parameter σ to θ in order to avoid confusing it with the standard deviation of the experimental results).

On the other hand, referring to the use of CMA-ES for solving our superimposition problem, some considerations have to be taken into account. Since we are dealing with a multimodal problem, we needed to adapt some parameter values to make

CMA-ES become appropriate to solve it. As said, in [26] the authors provide default values for all the set of parameters of the algorithm: $4 + \lfloor 3\ln(n) \rfloor$ for λ (with n being the number of genes) and $\lambda/2$ for μ. In our problem, $n = 12$, and thus $\lambda = 11$ and $\mu = 5$. We used these values but an unacceptable performance was achieved. However, in the same paper they recommend to enlarge λ and choose μ accordingly, to make the strategy more robust or more explorative in case of multimodality. So, after several preliminary experimentations testing different parameter values, we established their values to $\lambda = 100$ and $\mu = 15$ (very typical values in (μ, λ)-ESs but not in the CMA-ES), which were the ones that provided better results. Another problem, as in the case of the GA approaches, refers to the non-projectable solutions. For the already commented convergence problems, the initial solution, i.e. the one used to work out the initial distribution center $\langle \vec{x} \rangle_{\omega}^{(0)}$, is randomly generated until a set of transformation parameters corresponding to a projectable solution is obtained.

4.4. Binary-coded genetic algorithm

Finally, we considered Nickerson et al.'s approach [34] as a baseline to tackle the craniofacial superimposition problem. This decision was due to the fact that it is the only automatic proposal in the literature dealing with a 3D model of the skull and a photograph. In this proposal, the authors only indicated the use of a binary-coded genetic algorithm (BCGA), but they did not specified its components. Hence, in order to properly design the incomplete description we had to make several assumptions that were based on the date that contribution was published. In particular, we considered roulette-wheel selection, elitism, two point crossover and simple mutation operators [23] for the proposed binary-coded GA.

On the other hand, to make fairer the comparison between the designed algorithms, the same fitness function is considered and the initial population of the BCGA is generated as in the case of the RCGA.

5. Experiments

Our experimental study will involve three real-world cases previously addressed by the staff of the Physical Anthropology lab at the University of Granada in collaboration with the Spanish scientific police. Those three identification cases were solved following a computer supported but manual approach for photographic supra-projection. We will consider the 2D photographs of the missing people and their corresponding 3D skull models acquired at the lab by using its Konica-Minolta© 3D Lasserscanner VI-910. In this section, we first show the parameter setting considered in the experiments. Next, we present the three cases of study, the obtained results, and their analysis. Finally, we compare the manual superimpositions achieved by the forensic experts with those obtained by the EAs presented in this contribution.

5.1. Parameter setting

Referring to the experimental setup for the genetic approaches, we performed experiments with the following GA parameter values:

$$\begin{aligned}
&\text{generations} = 600\\
&\text{population size} = \{100; 500; 1000\}\\
&\text{crossover probability} = 0.9\\
&\text{mutation probability} = 0.2\\
&\text{tournament size(for RCGA)} = 2\\
&\text{BLX} - \alpha \text{ parameter(for RCGA)} = \{0.1, 0.3, 0.5, 0.7, 0.9\}\\
&\text{SBX}\eta\text{parameter(for RCGA)} = \{1, 2, 5, 10, 20\}
\end{aligned}$$

As can be seen, three different population sizes are tested for the three GAs as well as five values for the crossover operator parameter (establishing different exploration–exploitation trade-offs) for each of the two RCGAs.

In the case of CMA-ES, the following values were considered for the different parameters:

$$\begin{aligned}
&\text{evaluations} = \{55,200; 276,000; 552,000\}\\
&\text{initial } \theta \text{ (mutation distribution variance)} = \{0.00001, 0.0001, 0.001, 0.01, 0.1, 0.3\}\\
&\lambda \text{ (population size, offspring number)} = 100\\
&\mu \text{ (number of parents/points for recombination)} = 15
\end{aligned}$$

Notice that, in order to perform a fair comparison, the number of evaluations for the CMA-ES are those corresponding to the number of evaluations needed to perform 600 generations of a GA with 100, 500 and 1000 individuals, respectively, for the given mutation and crossover probabilities. Besides, six different values for the main CMA-ES parameter are also considered.

Regardless the specific parameter configuration for each proposed EA, there are some common considerations for all of them. Based on the values of the weighting coefficients (β_1, β_2), we can adjust the influence of the two error terms in the fitness function (Eq. (4)). In this work, we have considered three different choices: (1) $(\beta_1, \beta_2) = (1, 0)$: the resulting fitness

function becomes the same that the original one proposed by Nickerson et al., i.e. the mean distance between the corresponding landmarks; (2) $(\beta_1, \beta_2) = (0, 1)$: it corresponds to the maximum distance between the corresponding landmarks; (3) $(\beta_1, \beta_2) = (0.5, 0.5)$: it becomes the average of the two former ones.

In order to avoid execution dependence, thirty different runs for each parameter setting have been performed and different statistics are provided. We considered the MSE (see Eq. (5)) for the assessment of the final superimposition results.

Finally, all the methods are run on a PC with an AMD Athlon 64 X2 Dual (2 core 2.59 GHz), 2 GB of RAM and Linux CentOS.

5.2. Case study 1

The facial photograph of this missing lady found in Malaga, Spain, were provided by the family and the final identification done by photographic supra-projection has been confirmed. We studied this real case with the consent of the relatives. The 3D model of the skull, represented in the left image of Fig. 5, comprises 243,202 points (stored as x, y, z coordinates). The 2D image is a 290×371 RGB (red, green and blue) color image (see Fig. 5, right). The forensic experts manually selected a set of six 3D landmarks on the skull 3D model and their counterpart 2D landmarks on the face present in the photo, both shown in the left-most and right-most images in Fig. 5.

Table 1 shows the best results achieved by the implemented algorithms, BCGA, RCGA-BLX-α, RCGA-SBX, and CMA-ES, for the three given fitness function setups and for the different values of the parameters α, η and θ considered. In order to avoid overloading the reader with the large number of experimental results obtained and to ease the following of this section, the tables here included will only report those outcomes corresponding to the population size which caused the best performance for each of the considered EAs. All the remaining results are collected in the tables shown in Appendix A. For each algorithm, the best (m), the worst (M), the mean (μ), and the standard deviation (σ) values of the thirty runs are showed for the fitness, the MSE, and the MAX measures. The best values for the minimum and mean results for each fitness function parameter combination are highlighted in boldface. Notice that, statistics of the fitness are only comparable between the same combination of (β_1, β_2) values while statistics of the MSE and MAX are comparable all along the table. This table structure will be the one followed for all the tables in this Section 5 and in the corresponding Appendix A.

From the reported results in Table 1 (and from those in corresponding tables in Appendix A, Tables A.1–A.4) we can recognize how the fitness function $(\beta_1, \beta_2) = (1, 0)$ (that is to say, the MSE) is the one which achieved the best and the most robust results in every case. Concerning the fitness $(\beta_1, \beta_2) = (0.5, 0.5)$ we can assert its better performance when compared to $(\beta_1, \beta_2) = (0, 1)$. The only exception is the BCGA case, where the performance of both functions is quite similar.

Looking carefully at the BCGA results, we can see that the best performance is achieved when considering a 1000 individuals population. In addition, the poor robustness of the algorithm is clearly demonstrated. In spite of the best individual result reached, the results show high means and standard deviations. In the case of RCGA-BLX-α, 100 individuals and α values larger than 0.7 are the best configuration parameters. Anyway, it shows a low robustness (although higher than the BCGA), in view of the high means values.

Finally, the results obtained using RCGA-SBX and CMA-ES lead us to assert that they are clearly the best techniques for this identification case, with a very high robustness demonstrated by the fact that average values equal the minimum value. In the case of RCGA-SBX, the best performance is considered when using 1000 individuals and small values of η, that is, the opposite exploration–exploitation trade-off them in RCGA-BLX-α. CMA-ES also performs better with the largest number of evaluations, 552,000, but with high values of θ. Although the best individual results (minima) reached by the RCGA-SBX are the best ones overall, CMA-ES achieved very similar values and is less sensitive to the parameter setting. In fact, this algorithm always obtains the same minimum for all the parameter configurations tested using the MSE fitness.

Regarding to the visual results, the best superimpositions achieved are showed in Fig. 6. The 2D facial landmarks are represented by an "o" while the projected 3D cranial landmarks by an "x". Though the best results are quite similar for all the algorithms, this is not the case of the worst results, i.e. the worst run of the best parameter configuration (see Fig. 7). Notice that, in the case of BCGA and RCGA-BLX-α the skull has been downsized and it is located in the tip of the nose. Hence, results are only suitable for CMA-ES and RCGA-SBX.

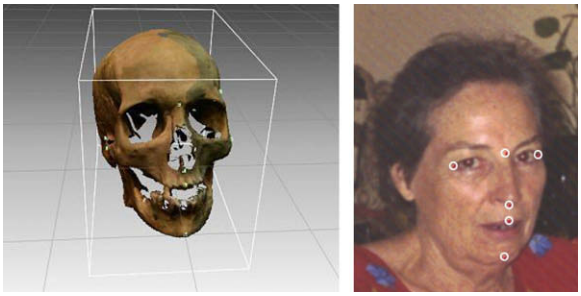

Fig. 5. Real-world case study 1: skull 3D model (left) and photograph of the missing person (right).

Table 1
Case study 1: superimposition results for the best performing population sizes.

β_1, β_2		Fitness				MSE				Max			
		m	M	μ	σ	m	M	μ	σ	m	M	μ	σ
BCGA (1000 individuals)													
1, 0		0.017	0.250	0.156	0.075	**0.017**	0.250	**0.156**	0.075	0.039	0.415	0.268	0.118
0, 1		0.094	0.372	0.298	0.073	0.075	0.272	0.220	0.052	0.094	0.372	0.298	0.073
0.5, 0.5		0.023	0.265	0.163	0.083	0.025	0.267	0.163	0.085	0.029	0.366	0.229	0.113
β_1, β_2	α	Fitness				MSE				Max			
		m	M	μ	σ	m	M	μ	σ	m	M	μ	σ
RCGA-BLX-α (100 individuals)													
1, 0	0.1	0.231	0.261	0.253	0.007	0.231	0.261	0.253	0.007	0.385	0.433	0.420	0.011
	0.3	0.233	0.262	0.254	0.007	0.233	0.262	0.254	0.007	0.387	0.434	0.422	0.011
	0.5	0.058	0.267	0.246	0.036	0.058	0.267	0.246	0.036	0.139	0.442	0.410	0.053
	0.7	0.020	0.237	0.080	0.074	**0.020**	0.237	**0.080**	0.074	0.030	0.376	0.129	0.116
	0.9	0.086	0.264	0.222	0.037	0.086	0.264	0.222	0.037	0.137	0.445	0.354	0.062
0, 1	0.1	0.340	0.380	0.363	0.008	0.249	0.273	0.265	0.005	0.340	0.380	0.363	0.008
	0.3	0.341	0.375	0.362	0.007	0.250	0.274	0.265	0.004	0.341	0.375	0.362	0.007
	0.5	0.310	0.375	0.361	0.013	0.227	0.273	0.264	0.009	0.310	0.375	0.361	0.013
	0.7	0.332	0.377	0.363	0.010	0.243	0.275	0.264	0.007	0.332	0.377	0.363	0.010
	0.9	0.153	0.381	0.347	0.054	**0.105**	0.276	**0.246**	0.045	0.153	0.381	0.347	0.054
0.5, 0.5	0.1	0.234	0.264	0.258	0.007	0.240	0.270	0.262	0.007	0.327	0.377	0.362	0.011
	0.3	0.246	0.266	0.259	0.006	0.250	0.271	0.264	0.006	0.343	0.372	0.362	0.008
	0.5	0.232	0.268	0.258	0.007	0.237	0.273	0.263	0.007	0.322	0.374	0.360	0.010
	0.7	0.022	0.269	0.163	0.100	**0.023**	0.273	**0.163**	0.101	0.030	0.375	0.230	0.139
	0.9	0.197	0.270	0.245	0.020	0.194	0.271	0.243	0.021	0.281	0.379	0.347	0.027
β_1, β_2	η	Fitness				MSE				Max			
		m	M	μ	σ	m	M	μ	σ	m	M	μ	σ
RCGA-SBX (1000 individuals)													
1, 0	1.0	0.016	0.020	0.018	0.001	**0.016**	0.020	**0.018**	0.001	0.036	0.056	0.051	0.004
	2.0	0.017	0.023	0.019	0.002	0.017	0.023	0.019	0.002	0.045	0.066	0.052	0.004
	5.0	0.016	0.044	0.024	0.006	**0.016**	0.044	0.024	0.006	0.031	0.155	0.055	0.021
	10.0	0.017	0.053	0.028	0.011	0.017	0.053	0.028	0.011	0.025	0.160	0.065	0.031
	20.0	0.017	0.062	0.034	0.012	0.017	0.062	0.034	0.012	0.034	0.183	0.080	0.037
0, 1	1.0	0.021	0.032	0.024	0.002	0.020	0.028	**0.023**	0.002	0.021	0.032	0.024	0.002
	2.0	0.022	0.048	0.029	0.008	0.021	0.046	0.027	0.007	0.022	0.048	0.029	0.008
	5.0	0.022	0.086	0.042	0.016	0.021	0.065	0.038	0.014	0.022	0.086	0.042	0.016
	10.0	0.023	0.088	0.051	0.018	**0.019**	0.070	0.044	0.015	0.023	0.088	0.051	0.018
	20.0	0.028	0.242	0.072	0.059	0.026	0.182	0.060	0.043	0.028	0.242	0.072	0.059
0.5, 0.5	1.0	0.017	0.028	0.019	0.002	**0.018**	0.029	**0.020**	0.002	0.023	0.038	0.025	0.003
	2.0	0.017	0.023	0.020	0.002	**0.018**	0.024	0.021	0.002	0.023	0.032	0.026	0.003
	5.0	0.017	0.048	0.026	0.009	**0.018**	0.056	0.027	0.010	0.023	0.058	0.034	0.011
	10.0	0.017	0.053	0.032	0.010	**0.018**	0.057	0.034	0.012	0.023	0.071	0.042	0.013
	20.0	0.019	0.086	0.041	0.018	0.021	0.087	0.041	0.016	0.024	0.120	0.059	0.029
β_1, β_2	θ	Fitness				MSE				Max			
		m	M	μ	σ	m	M	μ	σ	m	M	μ	σ
CMA-ES (552,000 evaluations)													
1, 0	0.00001	0.017	0.043	0.021	0.009	**0.017**	0.043	0.021	0.009	0.045	0.133	0.062	0.028
	0.00010	0.017	0.043	0.019	0.007	**0.017**	0.043	0.019	0.007	0.051	0.132	0.057	0.020
	0.00100	0.017	0.044	0.021	0.009	**0.017**	0.044	0.021	0.009	0.051	0.140	0.063	0.028
	0.01000	0.017	0.043	0.019	0.008	**0.017**	0.043	0.019	0.008	0.051	0.134	0.059	0.025
	0.10000	0.017	0.018	0.017	0.000	**0.017**	0.018	**0.017**	0.000	0.051	0.053	0.051	0.000
	0.30000	0.017	0.019	0.017	0.001	**0.017**	0.019	**0.017**	0.001	0.049	0.054	0.052	0.001
0, 1	0.00001	0.022	0.087	0.026	0.017	**0.021**	0.073	0.024	0.012	0.022	0.087	0.026	0.017
	0.00010	0.022	0.084	0.024	0.011	**0.021**	0.055	**0.022**	0.006	0.022	0.084	0.024	0.011
	0.00100	0.022	0.090	0.028	0.020	**0.021**	0.073	0.026	0.016	0.022	0.090	0.028	0.020
	0.01000	0.022	0.088	0.026	0.017	**0.021**	0.067	0.024	0.012	0.022	0.088	0.026	0.017
	0.10000	0.022	0.030	0.025	0.002	**0.021**	0.028	0.023	0.002	0.022	0.030	0.025	0.002
	0.30000	0.023	0.048	0.033	0.006	**0.021**	0.042	0.030	0.005	0.023	0.048	0.033	0.006
0.5, 0.5	0.00001	0.017	0.059	0.020	0.011	**0.018**	0.051	0.020	0.008	0.023	0.092	0.028	0.018
	0.00010	0.017	0.059	0.022	0.013	**0.018**	0.052	0.022	0.010	0.023	0.092	0.030	0.021
	0.00100	0.017	0.059	0.019	0.008	**0.018**	0.052	0.019	0.006	0.023	0.092	0.025	0.013
	0.01000	0.017	0.059	0.019	0.008	**0.018**	0.052	0.020	0.006	0.023	0.092	0.027	0.014
	0.10000	0.017	0.019	0.018	0.000	**0.018**	0.019	**0.018**	0.000	0.023	0.025	0.024	0.001
	0.30000	0.018	0.025	0.019	0.002	**0.018**	0.027	0.020	0.002	0.023	0.033	0.026	0.003

Fig. 6. Case study 1, from left to right: the best superimposition results obtained by means of BCGA, RCGA-BLX-α, RCGA-BSX, and CMA-ES are shown.

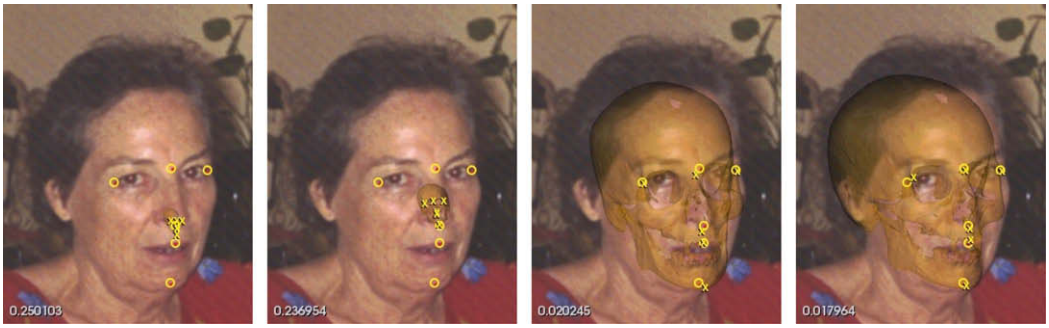

Fig. 7. Case study 1, from left to right: the worst superimposition results obtained with the best parameter configuration runs by means of BCGA, RCGA-BLX-α, RCGA-BSX, and CMA-ES are shown.

5.3. Case study 2

The 3D model of the skull (199,609 points stored as x, y, z coordinates) has been acquired by the aforementioned 3D range scanner, and the considered 2D photograph (1512×2243 RGB image) has been provided by the family.[2] The forensic anthropologists manually selected a set of six landmarks in both the skull and the photo.

The implemented algorithms have been applied to solve the superimposition problem using the same experimental setup of the previous case. Table 2 shows the best results obtained with the three fitness function settings.

In general, the conclusions drawn are quite similar to those obtained in the first case study. Results from BCGA are very little robust, presenting high variability. CMA-ES and RCGA-SBX are again the best performing algorithms and, for this case, RCGA-BLX-α achieves a similar performance.

From the results reported in Table 2 and the corresponding ones in Appendix A, (Tables A.5–A.8), it can be seen how, for all the configurations and algorithms, the fitness function weighting combination $(\beta_1, \beta_2) = (1, 0)$ is the one which produces the best and more robust results as well as that $(\beta_1, \beta_2) = (0.5, 0.5)$ performs better than $(\beta_1, \beta_2) = (0, 1)$. In every case, the best outcomes are obtained with the largest population size/evaluation number.

On the one hand, analyzing the BCGA results, the best results are achieved with 1000 individuals. As was already mentioned, we can see the low robustness of the algorithm in spite of a few good quality best individual results achieved. On the other hand, the performance of the two RCGAs is similar regardless the crossover operator used. For both possibilities and for the CMA-ES algorithm the results are outstanding. They all reach the same value for the best individual results (minimum), with very low means and standard deviations of zero or close to zero. As in the previous case, CMA-ES shows to be robust with respect to different configuration parameters with an slightly better performance for small and medium values of θ. Concerning RCGA-BLX-α, the best results are achieved in this case with $\alpha = 0.5$. For RCGA-SBX, better results are again achieved with low values of η.

5.4. Case study 3

This third case study is again a real-world one happened in Cadiz, Spain. The skull 3D model (327,641 points stored as x, y, z coordinates) was acquired by the aforementioned 3D range scanner. Two photographs were provided by the family. They were acquired at different moments and in different poses and conditions. Hence this case consists of two distinct

[2] Due to legal issues, we are not allowed to publish images of this case. Nevertheless, we will present and analyze numerical results.

Table 2
Case study 2: superimposition results for the best performing population sizes.

β_1, β_2		Fitness				MSE				MAX			
		m	M	μ	σ	m	M	μ	σ	m	M	μ	σ
BCGA (1000 individuals)													
1, 0		0.007	0.037	0.018	0.009	**0.007**	0.037	**0.018**	0.009	0.023	0.144	0.049	0.028
0, 1		0.013	0.337	0.073	0.088	**0.013**	0.272	**0.060**	0.071	0.013	0.337	0.073	0.088
0.5, 0.5		0.010	0.108	0.028	0.022	**0.010**	0.096	**0.027**	0.021	0.014	0.164	0.039	0.032
β_1, β_2	α	Fitness				MSE				MAX			
		m	M u	μ	σ	m	M	μ	σ	m	M	μ	σ
RCGA-BLX-α (1000 individuals)													
1, 0	0.1	0.029	0.081	0.063	0.011	0.029	0.081	0.063	0.011	0.058	0.195	0.131	0.031
	0.3	0.008	0.023	0.014	0.004	0.008	0.023	0.014	0.004	0.028	0.059	0.037	0.009
	0.5	0.007	0.009	0.008	0.001	**0.007**	0.009	**0.008**	0.001	0.026	0.030	0.029	0.001
	0.7	0.014	0.025	0.020	0.002	0.014	0.025	0.020	0.002	0.026	0.060	0.039	0.008
	0.9	0.060	0.141	0.099	0.022	0.060	0.141	0.099	0.022	0.090	0.339	0.199	0.063
0, 1	0.1	0.120	0.342	0.308	0.057	0.098	0.287	0.255	0.051	0.120	0.342	0.308	0.057
	0.3	0.053	0.341	0.201	0.097	0.039	0.286	0.162	0.087	0.053	0.341	0.201	0.097
	0.5	0.014	0.021	0.018	0.001	**0.012**	0.017	**0.014**	0.001	0.014	0.021	0.018	0.001
	0.7	0.027	0.047	0.037	0.005	0.018	0.035	0.025	0.004	0.027	0.047	0.037	0.005
	0.9	0.099	0.260	0.196	0.042	0.080	0.186	0.138	0.028	0.099	0.260	0.196	0.042
0.5, 0.5	0.1	0.053	0.099	0.077	0.012	0.049	0.087	0.071	0.009	0.070	0.160	0.117	0.025
	0.3	0.017	0.078	0.047	0.012	0.014	0.078	0.049	0.013	0.027	0.108	0.064	0.017
	0.5	0.010	0.013	0.012	0.001	**0.010**	0.013	**0.011**	0.001	0.015	0.019	0.017	0.001
	0.7	0.017	0.029	0.023	0.003	0.013	0.028	0.021	0.004	0.022	0.044	0.034	0.005
	0.9	0.069	0.161	0.124	0.023	0.065	0.155	0.117	0.024	0.102	0.250	0.181	0.033
β_1, β_2	η	Fitness				MSE				MAX			
		m	M	μ	σ	m	M	μ	σ	m	M	μ	σ
RCGA-SBX (1000 individuals)													
1, 0	1.0	0.007	0.008	0.008	0.000	**0.007**	0.008	**0.008**	0.000	0.019	0.028	0.025	0.003
	2.0	0.007	0.012	0.008	0.001	**0.007**	0.012	**0.008**	0.001	0.020	0.030	0.025	0.003
	5.0	0.007	0.017	0.009	0.002	**0.007**	0.017	0.009	0.002	0.016	0.043	0.024	0.007
	10.0	0.008	0.057	0.015	0.012	0.008	0.057	0.015	0.012	0.020	0.171	0.044	0.041
	20.0	0.008	0.085	0.028	0.022	0.008	0.085	0.028	0.022	0.019	0.271	0.072	0.060
0, 1	1.0	0.012	0.015	0.013	0.001	0.012	0.012	**0.012**	0.000	0.012	0.015	0.013	0.001
	2.0	0.012	0.023	0.014	0.002	0.012	0.019	0.013	0.001	0.012	0.023	0.014	0.002
	5.0	0.012	0.082	0.021	0.016	**0.011**	0.065	0.018	0.013	0.012	0.082	0.021	0.016
	10.0	0.013	0.091	0.038	0.022	0.012	0.079	0.033	0.019	0.013	0.091	0.038	0.022
	20.0	0.013	0.165	0.053	0.041	**0.011**	0.140	0.045	0.035	0.013	0.165	0.053	0.041
0.5, 0.5	1.0	0.009	0.011	0.010	0.000	**0.009**	0.011	**0.010**	0.000	0.013	0.016	0.014	0.000
	2.0	0.010	0.014	0.010	0.001	0.010	0.014	**0.010**	0.001	0.013	0.020	0.015	0.001
	5.0	0.010	0.060	0.015	0.010	0.010	0.046	0.014	0.008	0.013	0.102	0.021	0.017
	10.0	0.010	0.073	0.017	0.012	**0.009**	0.076	0.017	0.013	0.013	0.097	0.022	0.016
	20.0	0.010	0.083	0.028	0.020	**0.009**	0.091	0.027	0.019	0.014	0.114	0.039	0.030
β_1, β_2	θ	Fitness				MSE				MAX			
		m	M	μ	σ	m	M	μ	σ	m	M	μ	σ
CMA-ES (552,000 evaluations)													
1, 0	0.00001	0.007	0.018	0.008	0.002	**0.007**	0.018	0.008	0.002	0.019	0.042	0.025	0.004
	0.00010	0.007	0.091	0.010	0.015	**0.007**	0.091	0.010	0.015	0.019	0.234	0.031	0.038
	0.00100	0.007	0.091	0.010	0.015	**0.007**	0.091	0.010	0.015	0.020	0.233	0.031	0.038
	0.01000	0.007	0.008	0.007	0.000	**0.007**	0.008	**0.007**	0.000	0.020	0.027	0.025	0.002
	0.10000	0.007	0.098	0.014	0.019	**0.007**	0.098	0.014	0.019	0.025	0.309	0.041	0.053
	0.30000	0.007	0.251	0.065	0.088	**0.007**	0.251	0.065	0.088	0.020	0.430	0.114	0.137
0, 1	0.00001	0.012	0.012	0.012	0.000	**0.012**	0.012	**0.012**	0.000	0.012	0.012	0.012	0.000
	0.00010	0.012	0.012	0.012	0.000	**0.012**	0.012	**0.012**	0.000	0.012	0.012	0.012	0.000
	0.00100	0.012	0.012	0.012	0.000	**0.012**	0.012	**0.012**	0.000	0.012	0.012	0.012	0.000
	0.01000	0.012	0.012	0.012	0.000	**0.012**	0.012	**0.012**	0.000	0.012	0.012	0.012	0.000
	0.10000	0.012	0.310	0.065	0.080	**0.012**	0.230	0.047	0.056	0.012	0.310	0.065	0.080
	0.30000	0.012	0.357	0.195	0.131	**0.012**	0.276	0.140	0.095	0.012	0.357	0.195	0.131
0.5, 0.5	0.00001	0.010	0.010	0.010	0.000	**0.009**	0.010	**0.009**	0.000	0.013	0.014	0.014	0.000
	0.00010	0.010	0.010	0.010	0.000	**0.009**	0.010	**0.009**	0.000	0.014	0.015	0.014	0.000
	0.00100	0.010	0.021	0.010	0.002	**0.009**	0.019	0.010	0.002	0.013	0.031	0.014	0.003
	0.01000	0.010	0.010	0.010	0.000	**0.009**	0.010	**0.009**	0.000	0.013	0.014	0.014	0.000
	0.10000	0.010	0.238	0.066	0.081	0.010	0.226	0.062	0.077	0.014	0.358	0.095	0.117
	0.30000	0.010	0.270	0.135	0.095	0.010	0.273	0.126	0.093	0.014	0.367	0.195	0.134

superimposition problems. As we will describe in Section 5.5, the forensic experts tried to solve the case with both photographs but finally they were restricted to use only one of them. Fig. 8 depicts this data set.

The forensic anthropologists manually selected a large set of 3D landmarks on the skull. On the other hand, the 2D landmarks selected on the face photographs were eight and eleven, depending on the pose, as shown in Fig. 8. Indeed not all the landmarks are visible in all the poses. Of course, only the corresponding 3D–2D landmarks are used for solving the two superimposition problems.

Tables 3 and 4 (as well as Tables A.9–A.16 from Appendix A) show the results of this case for the two different photographs provided, with the parameter configurations used in the previous two cases of study.

In view of the latter results, we can recognize that, the best results were again obtained using the fitness settings $(\beta_1, \beta_2) = (1, 0)$, followed by $(\beta_1, \beta_2) = (0.5, 0.5)$ and $(\beta_1 \beta_2) = (0, 1)$ in descending order of performance. In every case but for RCGA-BLX-α, the best performance is obtained with the largest population size/evaluations number.

On the other hand, CMA-ES and RCGA-SBX are again the best choices for both poses. Their behavior is really robust: some means equal to the best individual values and many standard deviations vanish or are close to zero. As in the remaining cases, CMA-ES behaves properly for all the different values of the parameters. For RCGA-SBX, the best results are again obtained small values of η. The setting $\alpha = 0.7$ is the best one for RCGA-BLX-α.

When dealing with pose 1, the worst values for the best individual results correspond to RCGA-BLX-α, which is not able to reach the same minima as the remaining algorithms. Furthermore, it shows a lack of robust behavior. The BCGA is able to achieve similar best individual values to CMA-ES and RCGA-SBX. Nevertheless, means and standard deviations relative to BCGA are very high, even a little bit worse than RCGA-BLX-α.

The case of pose 2 is the opposite. The worst results are associated to BCGA. Indeed, it achieves the worst minima and the least robust behavior. Meanwhile, RCGA-BLX-α is able to reach the same or similar best minima as CMA-ES and RCGA-SBX. However, its means and standard deviations are quite high.

Figs. 9 and 10 show, respectively, the best and the corresponding worst superimpositions obtained by the implemented EAs for the first pose of the third case study. Figs. 11 and 12 are associated to the second pose.

Focusing on the first pose, we can see the good superimpositions achieved by the RCGA-SBX and the CMA-ES algorithms. Results from the other two algorithms are not good enough since the skull is too big, even bigger than the hair contour in the BCGA superimposition (see the left-most image in Fig. 9). When checking the worst superimpositions obtained for the best parameter combination runs (Fig. 10), we recognize how results from the first two algorithms (BCGA and RCGA-BLX-α) are absolutely unsuitable. The skull is again downsized around the nose, as it happened in the first case of study. However, those worst superimpositions corresponding to the other two EAs are acceptable. Notice that, they are as good as the best superimposition achieved by the BCGA in the case of RCGA-SBX, and even better than that achieved by RCGA-BLX-α in the case of CMA-ES.

Concerning the second pose of this case, we should remind that, 11 landmarks were selected by the anthropologists, which is a higher number of landmarks than those in all the previous cases. Nevertheless, very similar conclusions can be drawn. Good superimpositions are achieved (see Fig. 11), even in the case of BCGA. However, superimpositions corresponding to the worst of the 30 runs (see Fig. 12), are only acceptable for RCGA-SBX and CMA-ES.

5.5. Benchmarking of the EA-based superimpositions with respect to the forensic anthropologists' ones

EAs are being increasingly applied to difficult real-world problems [3,31,48] and they are becoming competitive to the work done by creative and inventive human beings day by day, as attested by the "*annual HUMIES awards for human-competitive results produced by genetic and evolutionary computation*" [1].

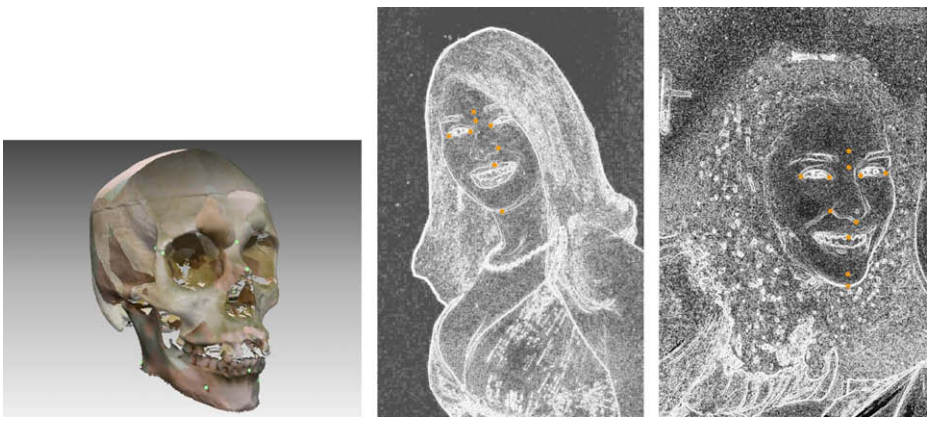

Fig. 8. Case study 3, from left to right: 3D model of the skull and two photographs of the missing person in different poses are shown. Notice that we have processed the photographs to hide the subject identity following legal issues.

Table 3
Case study 3, pose 1: superimposition results for the best performing population sizes.

β_1, β_2		Fitness				MSE				MAX			
		m	M	μ	σ	m	M	μ	σ	m	M	μ	σ
BCGA (1000 individuals)													
1, 0		0.017	0.128	0.072	0.036	**0.017**	0.128	**0.072**	0.036	0.035	0.341	0.194	0.099
0, 1		0.037	0.231	0.132	0.063	**0.024**	0.164	**0.094**	0.044	0.037	0.231	0.132	0.063
0.5, 0.5		0.023	0.145	0.091	0.044	**0.022**	0.140	**0.086**	0.042	0.030	0.202	0.129	0.062
β_1, β_2	α	Fitness				MSE				MAX			
		m	M	μ	σ	m	M	μ	σ	m	M	μ	σ
RCGA-BLX-α (100 individuals)													
1, 0	0.1	0.111	0.130	0.124	0.005	0.111	0.130	0.124	0.005	0.304	0.348	0.332	0.012
	0.3	0.065	0.131	0.119	0.014	0.065	0.131	0.119	0.014	0.153	0.347	0.319	0.040
	0.5	0.036	0.122	0.075	0.028	0.036	0.122	0.075	0.028	0.078	0.331	0.204	0.079
	0.7	0.022	0.094	0.053	0.022	**0.022**	0.094	**0.053**	0.022	0.039	0.259	0.137	0.070
	0.9	0.051	0.121	0.100	0.015	0.051	0.121	0.100	0.015	0.077	0.331	0.247	0.050
0, 1	0.1	0.204	0.228	0.217	0.006	0.147	0.166	0.157	0.004	0.204	0.228	0.217	0.006
	0.3	0.185	0.226	0.216	0.008	0.136	0.163	0.155	0.005	0.185	0.226	0.216	0.008
	0.5	0.068	0.226	0.205	0.037	0.043	0.162	0.145	0.027	0.068	0.226	0.205	0.037
	0.7	0.034	0.225	0.176	0.055	**0.025**	0.165	**0.124**	0.040	0.034	0.225	0.176	0.055
	0.9	0.121	0.225	0.186	0.024	0.094	0.158	0.132	0.017	0.121	0.225	0.186	0.024
0.5, 0.5	0.1	0.148	0.169	0.161	0.005	0.138	0.158	0.151	0.005	0.199	0.227	0.216	0.006
	0.3	0.093	0.169	0.158	0.015	0.089	0.157	0.147	0.014	0.121	0.225	0.211	0.021
	0.5	0.024	0.169	0.120	0.057	0.023	0.158	0.111	0.052	0.031	0.226	0.161	0.077
	0.7	0.026	0.156	0.076	0.043	**0.022**	0.144	**0.063**	0.039	0.035	0.217	0.111	0.062
	0.9	0.092	0.147	0.127	0.016	0.065	0.136	0.105	0.019	0.123	0.249	0.188	0.029
β_1, β_2	η	Fitness				MSE				MAX			
		m	M	μ	σ	m	M	μ	σ	m	M	μ	σ
RCGA-SBX (1000 individuals)													
1, 0	1.0	0.015	0.020	0.015	0.001	**0.015**	0.020	**0.015**	0.001	0.035	0.044	0.040	0.002
	2.0	0.015	0.032	0.016	0.003	**0.015**	0.032	0.016	0.003	0.038	0.086	0.042	0.008
	5.0	0.015	0.037	0.018	0.005	**0.015**	0.037	0.018	0.005	0.034	0.113	0.043	0.017
	10.0	0.015	0.037	0.023	0.007	**0.015**	0.037	0.023	0.007	0.034	0.160	0.059	0.031
	20.0	0.016	0.040	0.026	0.007	0.016	0.040	0.026	0.007	0.034	0.123	0.068	0.028
0, 1	1.0	0.028	0.053	0.031	0.006	0.022	0.041	0.026	0.007	0.028	0.053	0.031	0.006
	2.0	0.028	0.044	0.030	0.004	0.022	0.041	**0.024**	0.005	0.028	0.044	0.030	0.004
	5.0	0.028	0.059	0.036	0.009	0.021	0.051	0.030	0.009	0.028	0.059	0.036	0.009
	10.0	0.029	0.066	0.043	0.012	**0.020**	0.054	0.035	0.011	0.029	0.066	0.043	0.012
	20.0	0.031	0.181	0.052	0.034	0.023	0.133	0.041	0.025	0.031	0.181	0.052	0.034
0.5, 0.5	1.0	0.021	0.035	0.021	0.003	**0.016**	0.039	**0.017**	0.004	0.031	0.040	0.032	0.002
	2.0	0.021	0.036	0.023	0.005	**0.016**	0.039	0.019	0.007	0.030	0.043	0.033	0.004
	5.0	0.021	0.040	0.026	0.007	**0.016**	0.041	0.025	0.009	0.029	0.049	0.035	0.006
	10.0	0.021	0.048	0.029	0.008	0.017	0.050	0.028	0.009	0.029	0.058	0.038	0.009
	20.0	0.021	0.058	0.031	0.010	0.017	0.054	0.030	0.010	0.029	0.077	0.040	0.011
β_1, β_2	θ	Fitness				MSE				MAX			
		m	M	μ	σ	m	M	μ	σ	m	M	μ	σ
CMA-ES (552,000 evaluations)													
1, 0	0.00001	0.015	0.032	0.016	0.003	**0.015**	0.032	0.016	0.003	0.040	0.086	0.042	0.008
	0.00010	0.015	0.015	0.015	0.000	**0.015**	0.015	**0.015**	0.000	0.040	0.041	0.040	0.000
	0.00100	0.015	0.032	0.016	0.004	**0.015**	0.032	0.016	0.004	0.040	0.085	0.043	0.011
	0.01000	0.015	0.032	0.017	0.006	**0.015**	0.032	0.017	0.006	0.040	0.086	0.046	0.016
	0.10000	0.015	0.015	0.015	0.000	**0.015**	0.015	**0.015**	0.000	0.040	0.041	0.040	0.000
	0.30000	0.015	0.079	0.023	0.018	**0.015**	0.079	0.023	0.018	0.034	0.219	0.055	0.039
0, 1	0.00001	0.028	0.058	0.030	0.006	**0.022**	0.044	0.025	0.005	0.028	0.058	0.030	0.006
	0.00010	0.028	0.058	0.034	0.009	**0.022**	0.044	0.029	0.008	0.028	0.058	0.034	0.009
	0.00100	0.028	0.059	0.032	0.008	**0.022**	0.045	0.027	0.008	0.028	0.059	0.032	0.008
	0.01000	0.028	0.058	0.032	0.007	**0.022**	0.044	0.027	0.007	0.028	0.058	0.032	0.007
	0.10000	0.028	0.029	0.028	0.000	**0.022**	0.024	**0.023**	0.001	0.028	0.029	0.028	0.000
	0.30000	0.028	0.128	0.046	0.028	**0.022**	0.083	0.034	0.018	0.028	0.128	0.046	0.028
0.5, 0.5	0.00001	0.021	0.045	0.025	0.008	**0.016**	0.044	0.023	0.010	0.031	0.058	0.035	0.006
	0.00010	0.021	0.045	0.024	0.007	**0.016**	0.044	0.020	0.009	0.031	0.058	0.034	0.006
	0.00100	0.021	0.047	0.024	0.008	**0.016**	0.046	0.021	0.010	0.031	0.060	0.034	0.008
	0.01000	0.021	0.036	0.023	0.005	**0.016**	0.039	0.019	0.008	0.031	0.042	0.033	0.003
	0.10000	0.021	0.022	0.021	0.000	**0.016**	0.017	**0.016**	0.000	0.031	0.033	0.031	0.000
	0.30000	0.021	0.103	0.033	0.023	**0.016**	0.095	0.028	0.022	0.031	0.137	0.047	0.031

Table 4
Case study 3, pose 2: superimposition results for the best performing population sizes.

β_1, β_2		Fitness				MSE				MAX			
		m	M	μ	σ	m	M	μ	σ	m	M	μ	σ
BCGA (1000 individuals)													
1, 0		0.039	0.157	0.092	0.034	**0.039**	0.157	**0.092**	0.034	0.107	0.324	0.187	0.063
0, 1		0.096	0.279	0.189	0.063	**0.060**	0.197	**0.133**	0.044	0.096	0.279	0.189	0.063
0.5, 0.5		0.066	0.190	0.128	0.039	**0.052**	0.183	**0.122**	0.039	0.092	0.262	0.179	0.053
β_1, β_2	α	Fitness				MSE				MAX			
		m	M	μ	σ	m	M	μ	σ	m	M	μ	σ
RCGA-BLX-α (100 individuals)													
1, 0	0.1	0.145	0.188	0.172	0.011	0.145	0.188	0.172	0.011	0.295	0.401	0.364	0.027
	0.3	0.060	0.187	0.159	0.035	0.060	0.187	0.159	0.035	0.123	0.399	0.335	0.074
	0.5	0.036	0.063	0.052	0.009	**0.036**	0.063	**0.052**	0.009	0.106	0.149	0.128	0.013
	0.7	0.038	0.094	0.052	0.017	0.038	0.094	**0.052**	0.017	0.114	0.220	0.143	0.019
	0.9	0.095	0.164	0.131	0.019	0.095	0.164	0.131	0.019	0.177	0.387	0.278	0.053
0, 1	0.1	0.251	0.289	0.279	0.008	0.176	0.210	0.201	0.007	0.251	0.289	0.279	0.008
	0.3	0.249	0.292	0.278	0.009	0.169	0.210	0.198	0.008	0.249	0.292	0.278	0.009
	0.5	0.129	0.292	0.245	0.052	0.065	0.205	0.168	0.044	0.129	0.292	0.245	0.052
	0.7	0.099	0.261	0.133	0.052	**0.060**	0.185	**0.085**	0.037	0.099	0.261	0.133	0.052
	0.9	0.137	0.276	0.230	0.037	0.085	0.194	0.159	0.028	0.137	0.276	0.230	0.037
0.5, 0.5	0.1	0.171	0.206	0.196	0.008	0.168	0.202	0.192	0.008	0.239	0.288	0.274	0.011
	0.3	0.130	0.209	0.196	0.016	0.115	0.204	0.190	0.018	0.197	0.290	0.273	0.021
	0.5	0.062	0.205	0.143	0.058	**0.044**	0.199	0.134	0.063	0.106	0.284	0.207	0.072
	0.7	0.063	0.161	0.083	0.026	0.045	0.150	**0.069**	0.028	0.107	0.235	0.131	0.034
	0.9	0.098	0.183	0.153	0.023	0.081	0.176	0.141	0.024	0.152	0.276	0.221	0.032
β_1, β_2	η	Fitness				MSE				MAX			
		m	M	μ	σ	m	M	μ	σ	m	M	μ	σ
RCGA-SBX (1000 individuals)													
1, 0	1.0	0.036	0.037	0.036	0.000	**0.036**	0.037	**0.036**	0.000	0.141	0.146	0.144	0.001
	2.0	0.036	0.037	0.036	0.000	**0.036**	0.037	**0.036**	0.000	0.141	0.145	0.144	0.001
	5.0	0.036	0.057	0.040	0.007	**0.036**	0.057	0.040	0.007	0.112	0.156	0.141	0.010
	10.0	0.036	0.061	0.046	0.009	**0.036**	0.061	0.046	0.009	0.107	0.236	0.140	0.025
	20.0	0.036	0.068	0.051	0.009	**0.036**	0.068	0.051	0.009	0.113	0.196	0.145	0.021
0, 1	1.0	0.090	0.105	0.094	0.005	0.062	0.079	**0.068**	0.003	0.090	0.105	0.094	0.005
	2.0	0.089	0.105	0.095	0.006	0.061	0.073	**0.068**	0.003	0.089	0.105	0.095	0.006
	5.0	0.090	0.108	0.099	0.006	**0.059**	0.075	**0.068**	0.004	0.090	0.108	0.099	0.006
	10.0	0.090	0.118	0.102	0.006	0.061	0.096	0.070	0.007	0.090	0.118	0.102	0.006
	20.0	0.094	0.192	0.109	0.017	0.060	0.130	0.073	0.013	0.094	0.192	0.109	0.017
0.5, 0.5	1.0	0.062	0.067	0.063	0.002	0.043	0.061	**0.046**	0.005	0.091	0.109	0.105	0.004
	2.0	0.062	0.067	0.063	0.002	**0.042**	0.062	0.047	0.007	0.091	0.111	0.105	0.006
	5.0	0.062	0.078	0.065	0.003	**0.042**	0.073	0.049	0.008	0.092	0.110	0.107	0.004
	10.0	0.062	0.075	0.067	0.003	0.043	0.069	0.055	0.008	0.093	0.111	0.106	0.005
	20.0	0.063	0.084	0.068	0.004	0.043	0.079	0.056	0.009	0.098	0.118	0.106	0.004
β_1, β_2	θ	Fitness				MSE				MAX			
		m	M	μ	σ	m	M	μ	σ	m	M	μ	σ
CMA-ES (552,000 evaluations)													
1, 0	0.00001	0.036	0.036	0.036	0.000	**0.036**	0.036	**0.036**	0.000	0.144	0.145	0.145	0.000
	0.00010	0.036	0.061	0.037	0.005	**0.036**	0.061	0.037	0.005	0.144	0.169	0.145	0.004
	0.00100	0.036	0.036	0.036	0.000	0.036	**0.036**	**0.036**	0.000	0.144	0.145	0.145	0.000
	0.01000	0.036	0.062	0.037	0.005	**0.036**	0.062	0.037	0.005	0.144	0.179	0.146	0.006
	0.10000	0.036	0.036	0.036	0.000	**0.036**	0.036	**0.036**	0.000	0.144	0.145	0.145	0.000
	0.30000	0.036	0.092	0.038	0.010	**0.036**	0.092	0.038	0.010	0.132	0.194	0.146	0.009
0, 1	0.00001	0.089	0.108	0.098	0.007	**0.063**	0.074	0.068	0.004	0.089	0.108	0.098	0.007
	0.00010	0.089	0.108	0.100	0.007	**0.063**	0.074	0.068	0.004	0.089	0.108	0.100	0.007
	0.00100	0.089	0.108	0.097	0.006	**0.063**	0.074	**0.066**	0.003	0.089	0.108	0.097	0.006
	0.01000	0.089	0.108	0.098	0.007	**0.063**	0.074	0.068	0.004	0.089	0.108	0.098	0.007
	0.10000	0.089	0.100	0.091	0.003	0.065	0.071	0.069	0.001	0.089	0.100	0.091	0.003
	0.30000	0.089	0.176	0.098	0.021	**0.063**	0.124	0.070	0.011	0.089	0.176	0.098	0.021
0.5, 0.5	0.00010	0.062	0.078	0.064	0.005	0.044	0.073	0.050	0.010	0.092	0.110	0.105	0.005
	0.00100	0.062	0.077	0.064	0.004	**0.042**	0.073	0.049	0.008	0.092	0.110	0.105	0.004
	0.01000	0.062	0.067	0.063	0.002	0.044	0.062	0.049	0.007	0.092	0.107	0.103	0.006
	0.10000	0.062	0.062	0.062	0.000	0.044	0.044	**0.044**	0.000	0.106	0.107	0.106	0.000
	0.30000	0.062	0.077	0.063	0.003	0.043	0.065	0.047	0.007	0.091	0.117	0.105	0.006

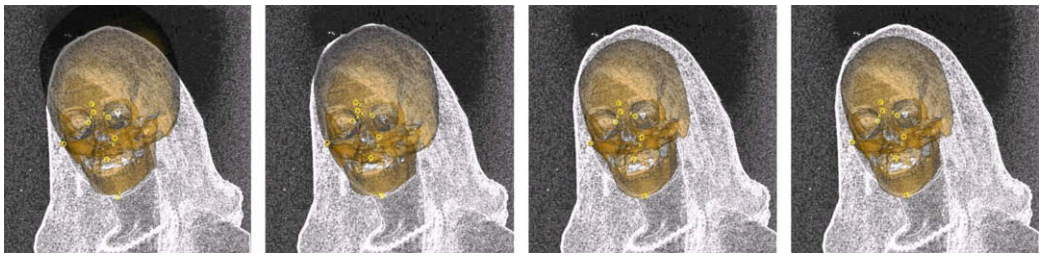

Fig. 9. Case study 3, pose 1. From left to right: the best superimposition results obtained by BCGA, RCGA-BLX-α, RCGA-SBX, and CMA-ES are shown.

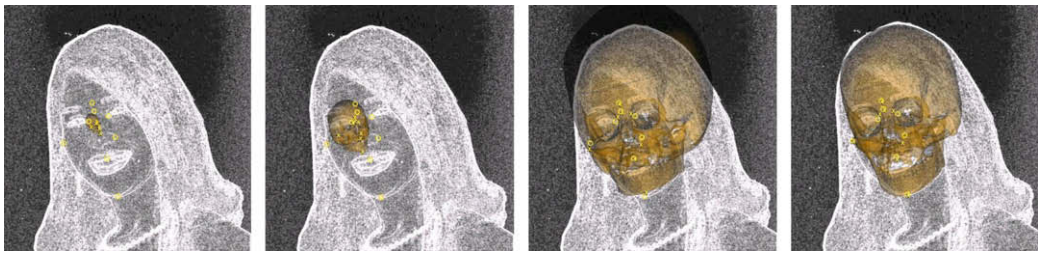

Fig. 10. Case study 3, pose 1. From left to right: the worst superimposition results obtained by BCGA, RCGA-BLX-α, RCGA-SBX, and CMA-ES are shown.

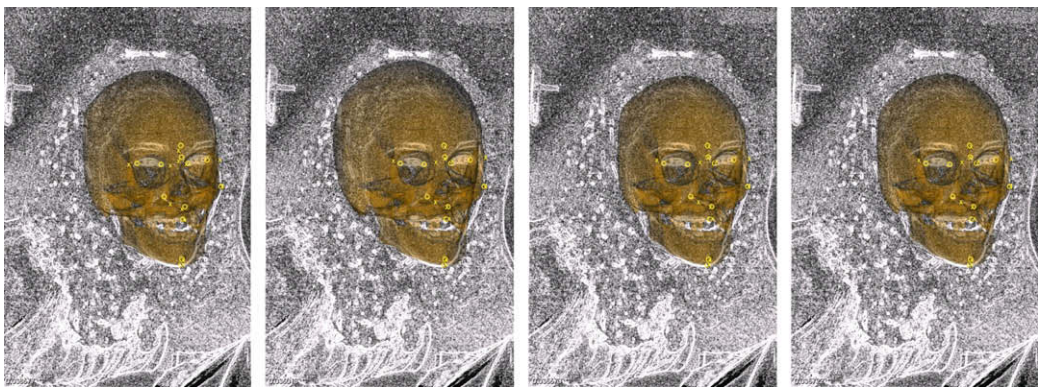

Fig. 11. Case study 3, pose 2. From left to right: the best superimposition results obtained by BCGA, RCGA-BLX-α, RCGA-SBX, and CMA-ES are shown.

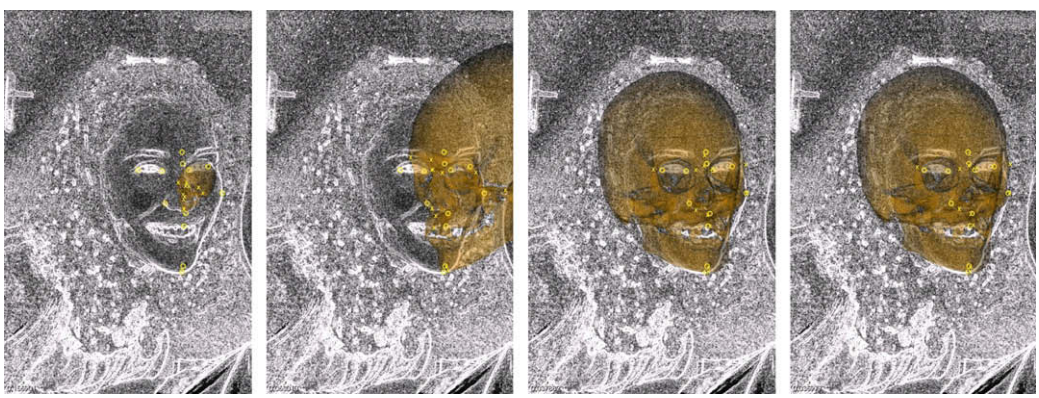

Fig. 12. Case study 3, pose 2. From left to right: worst superimposition results obtained by BCGA, RCGA-BLX-α, RCGA-SBX, and CMA-ES are shown.

The aim of this section is to evaluate the actual performance of the automatic craniofacial superimpositions of real-world forensic identification cases obtained using the evolutionary methodology introduced in this contribution. To do so, we will compare them to the manual (in fact, computer-assisted) superimpositions the forensic experts developed for the said cases. The comparison procedure established can be mainly based in two key aspects, the quality of the superimpositions and the time needed to obtain them.

In order to analyze the human-competitiveness of the superimpositions quality, we should first mention that, although comparing two graphical results is always a subjective issue, we benefit from having an available experienced forensic team to validate our results. Besides, any non-expert reader can even directly perform his own visual comparison of the human and EA-based superimpositions when they are represented in two consecutive images. We have always considered the output of the CMA-ES algorithm for the automatic craniofacial superimpositions shown in this section since, as shown in the previous subsections, it seems to be the most robust approach.

The left image in Fig. 13 shows the final superimposition used by the forensic experts at the University of Granada, Spain, to take a positive identification decision for that case in the past. The right image in the same figure depicts the best superimposition obtained by CMA-ES for the first case study considered. A direct inspection of both images allows us to recognize the large similarity among them. It is true that the automatic superimposition seems to be slightly excessively rotated to the left but also that the human superimposition is not properly "matching" the right part of the face (notice how the right side of the skull does not properly reach the cheek and ear level). When we provided the forensic anthropologists with our superimposition and asked them about this fact, they first recognized the defects of their superimposition. The forensic scientists explained to us that these defects are due the limitations of the perspective transformations they can obtain when projecting the 3D skull into a 2D image with the commercial software used (see Section 2.2). They mentioned how their main interest when performing the superimposition is always headed to properly match the main landmarks in the frontal horizontal and vertical axis, and that small misalignments in other parts of the face could be allowed. Then, they told us that our automatic superimposition was of high quality and that it would become definitively better than theirs after a little manual refinement.

Fig. 14 shows the same graphical comparison for the first pose of the third case study tackled. Now, even a non-expert reader can directly recognize the high similarity between the two superimpositions, which present exactly the same pose, and how ours achieves a better fit of the top part of the head thanks to our better treatment of the perspective transformation. That fact was confirmed by the forensic experts, *which preferred our superimposition to theirs*.

Finally, the most impressive outcome was that of the second pose of case study 3. This identification problem constitutes a particularly difficult situation for the forensic anthropologist since the more frontal the pose of the person in the photo-

Fig. 13. Case study 1, best superimposition manually obtained by the forensic experts (left) and automatic one achieved by means of CMA-ES (right).

Fig. 14. Case study 3, pose 1, best superimposition manually obtained by the forensic experts (left) and automatic one achieved by means of CMA-ES (right).

Fig. 15. Case study 3, pose 2, best superimposition manually obtained by the forensic experts (left) and automatic one achieved by means of CMA-ES (right).

graph, the more robust and easily applicable the technique. Notice that, the pose of the young woman in the second available photograph for this case (right-most image in Fig. 8) is very lateral. Thus, they deal with significant perspective deformations causing a lower confidence on the extracted landmarks (as said, this is the case for which a highest number of facial landmarks were selected). The left image in Fig. 15 shows the superimposition the forensic experts managed to get when they solved this case. As can be seen, although they were able to fit the frontal axis (see the proper alignment of the jaw and the eye caves), the skull is clearly downsized and the top and right parts of the face do not properly fit. This is again a consequence of the limitations of the considered software, even more noticeable in this case than in case study 1. That was the reason why the current photograph was finally ignored for the positive identification performed, that was confirmed by only considering the previous picture.

Nevertheless, the outstanding quality of the obtained evolutionary-based superimposition, depicted in the right image of Fig. 15, can be clearly seen. Not only the frontal axis but also the outer parts of the face (the forehead and the right cheek) are properly aligned, thanks to the said better handling of the perspective projection. Actually, *the forensic experts were positively impressed by the quality of that superimposition*.

On the other hand, we have not already mentioned anything about the run time of the different evolutionary approaches considered. Though this time differs for each EA, one execution of the two RCGAs designed ranges [0.8, 1.0] s for a population size of 100 individuals, [4.5, 5.0] s for 500 individuals, and [9.0, 10.0] for 1000 individuals. For the BCGA, run times range from [1.6, 1.8] s for 100 individual populations and [8, 9] s for 500 individuals, to [16.0,18.0] s for 1000 individuals. Finally, in the case of CMA-ES, the average run time is [1.5, 1.7] s when it develops 55,200 evaluations, [7.5, 8.5] s for 276,000 evaluations, and [15.0, 17.0] s for 552,000 evaluations. Hence, the RCGA approaches are the fastest ones, being the run times of the other two EAs very similar between them.

Anyway, comparing these times with the ones our forensic experts needed to perform each of the three said identifications – around 24 h for each case – the evolutionary approaches are always much better, lower in several orders of magnitude. Due to that, apart from their already analyzed quality, new outlooks in forensic identification could emerge. On the one hand, our proposal could be considered as a very fast initialization to provide a high quality craniofacial superimposition to be later slightly refined by the forensic scientist, in a very simple and quick way. On the other hand, the chance of comparing a skull 3D model with a large data base of missing people arises, taking the same or less time than an anthropologist would need to perform a single craniofacial superimposition.

6. Concluding remarks and future works

The aim of our project is to design a complete, automatic, soft computing-based procedure to aid the forensic anthropologist in the identification task by photographic supra-projection. In this paper, we have proposed and validated the use of real-coded EAs for the craniofacial superimposition stage of the process which involves the alignment/registration of the 3D skull model with the 2D face photograph of the missing person. The proposed methods are fast (they always take less than 18 s), robust and fully automatic, and therefore very useful for solving one of the most tedious activities (requiring around 24 h per case) performed by the forensic anthropologists. In addition, our method supposed a systematic approach to solve the superimposition problem and, in spite of it still needs some improvements, it could be used now as a tool for automatically obtaining a good quality superimposition to be manually refined by the forensic expert in a quick way.

We have presented and discussed superimposition results obtained on three real-world identification cases. A large number of experiments to analyze the influence of the parameter values has been performed. Our good results show a large

improvement of our methods with respect to our implementation of the original BCGA proposed by Nickerson et al. [34], that did not successfully work on our data. Results from RCGA-BLX-α seem not to be suitable mainly due to their high variability. RCGA-SBX and especially CMA-ES have a good performance, achieving high quality solutions in all the cases and showing a high robustness.

Craniofacial superimposition is a very challenging problem for several reasons. As we have already shown, most of the landmarks are nearly coplanar, making the system of equations undetermined. Moreover, we should notice the large range of the parameters we used, in order to consider one of the worst possible settings of the camera. This makes the search space of the EA much bigger than any possible real identification problem. One important future work is initializing the algorithm and restricting the parameter ranges using problem specific information (domain knowledge) [42]. Moreover, we should remind that we are dealing with real craniofacial superimposition cases, where the thickness of the soft tissue, as well as the uncertainty of localizing landmarks, influence the final results of our automatic evolutionary approach. We have started working in this line proposing a first approach to the location uncertainty problem [29] and we are planning to tackle the matching uncertainty in the short future.

We are also planning to automate the landmark extraction [42,53]. Moreover, we aim to consider a higher number of real cases of identification provided and solved by the Physical Anthropology lab at the University of Granada, as well as negative cases.

Finally, we aim to tackle the third identification stage, i.e. the decision making, by using fuzzy reasoning models in order to assist the forensic expert to take the final identification decision.

Acknowledgements

This work is supported by the Spanish Ministerio de Educación y Ciencia (Ref. TIN2006-00829) and by the Andalusian Dpt. of Innovación, Ciencia y Empresa (Ref. TIC-1619), both including EDRF fundings. We want to acknowledge all the team of the Physical Anthropology lab at the University of Granada (headed by Dr. Botella and Dr. Alemán) for their support during the data acquisition and validation processes. Especially, the authors would like to thank the anonymous referees for their valuable comments that allowed us to highly improve the paper quality. Part of the experiments related to this work was supported by the computing resources at the Supercomputation Center of Galicia (CESGA), Spain.

Appendix A. Experimentation results

See Tables A.1–A.16.

Table A.1
Case study 1: superimposition results for the BCGA algorithm.

β_1, β_2	Pop size	Fitness				MSE				MAX			
		m	M	μ	σ	m	M	μ	σ	m	M	μ	σ
1, 0	100	0.156	0.268	0.241	0.026	0.156	0.268	0.241	0.026	0.289	0.446	0.404	0.035
	500	0.021	0.262	0.171	0.074	0.021	0.262	0.171	0.074	0.044	0.434	0.289	0.122
0, 1	100	0.244	0.420	0.359	0.037	0.188	0.284	0.262	0.024	0.244	0.420	0.359	0.037
	500	0.025	0.373	0.289	0.097	0.021	0.272	0.214	0.069	0.025	0.373	0.289	0.097
0.5, 0.5	100	0.039	0.282	0.246	0.049	0.044	0.278	0.250	0.049	0.050	0.410	0.344	0.071
	500	0.020	0.269	0.203	0.080	0.021	0.273	0.206	0.082	0.028	0.374	0.283	0.111

Table A.2
Case study 1: superimposition results for the RCGA-BLX-α algorithm.

β_1, β_2	Pop size	α	Fitness				MSE				MAX			
			m	M	μ	σ	m	M	μ	σ	m	M	μ	σ
1, 0	500	0.1	0.221	0.257	0.250	0.009	0.221	0.257	0.250	0.009	0.336	0.426	0.412	0.022
		0.3	0.138	0.259	0.246	0.025	0.138	0.259	0.246	0.025	0.251	0.429	0.409	0.038
		0.5	0.065	0.259	0.242	0.037	0.065	0.259	0.242	0.037	0.125	0.430	0.400	0.059
		0.7	0.035	0.242	0.165	0.060	0.035	0.242	0.165	0.060	0.078	0.399	0.273	0.097
		0.9	0.179	0.255	0.228	0.021	0.179	0.255	0.228	0.021	0.241	0.537	0.374	0.051
	1000	0.1	0.238	0.257	0.252	0.004	0.238	0.257	0.252	0.004	0.383	0.425	0.416	0.009
		0.3	0.068	0.258	0.227	0.055	0.068	0.258	0.227	0.055	0.137	0.427	0.375	0.091
		0.5	0.108	0.256	0.223	0.045	0.108	0.256	0.223	0.045	0.120	0.425	0.366	0.081
		0.7	0.115	0.242	0.197	0.037	0.115	0.242	0.197	0.037	0.192	0.412	0.324	0.062
		0.9	0.110	0.246	0.208	0.038	0.110	0.246	0.208	0.038	0.146	0.410	0.338	0.068

(continued on next page)

Table A.2 (*continued*)

β_1, β_2	Pop size	α	Fitness				MSE				MAX			
			m	M	μ	σ	m	M	μ	σ	m	M	μ	σ
0, 1	500	0.1	0.331	0.368	0.362	0.007	0.238	0.269	0.265	0.005	0.331	0.368	0.362	0.007
		0.3	0.244	0.368	0.360	0.022	0.174	0.269	0.263	0.017	0.244	0.368	0.360	0.022
		0.5	0.234	0.370	0.352	0.036	0.118	0.270	0.255	0.034	0.234	0.370	0.352	0.036
		0.7	0.334	0.376	0.366	0.011	0.231	0.274	0.265	0.012	0.334	0.376	0.366	0.011
		0.9	0.314	0.379	0.359	0.014	0.217	0.276	0.256	0.013	0.314	0.379	0.359	0.014
	1000	0.1	0.358	0.366	0.363	0.002	0.260	0.268	0.265	0.002	0.358	0.366	0.363	0.002
		0.3	0.361	0.367	0.364	0.002	0.264	0.268	0.266	0.001	0.361	0.367	0.364	0.002
		0.5	0.211	0.368	0.357	0.031	0.149	0.269	0.259	0.027	0.211	0.368	0.357	0.031
		0.7	0.265	0.372	0.361	0.023	0.187	0.271	0.261	0.021	0.265	0.372	0.361	0.023
		0.9	0.280	0.371	0.346	0.025	0.172	0.269	0.243	0.027	0.280	0.371	0.346	0.025
0.5, 0.5	500	0.1	0.233	0.263	0.258	0.005	0.239	0.267	0.262	0.005	0.324	0.368	0.361	0.008
		0.3	0.219	0.264	0.257	0.009	0.195	0.269	0.259	0.016	0.347	0.369	0.362	0.005
		0.5	0.200	0.265	0.256	0.015	0.202	0.269	0.259	0.016	0.279	0.369	0.357	0.021
		0.7	0.217	0.262	0.244	0.013	0.201	0.267	0.242	0.019	0.315	0.379	0.349	0.016
		0.9	0.108	0.269	0.233	0.042	0.099	0.272	0.230	0.044	0.164	0.380	0.332	0.055
	1000	0.1	0.233	0.262	0.255	0.008	0.231	0.266	0.258	0.010	0.330	0.367	0.359	0.009
		0.3	0.124	0.262	0.249	0.031	0.109	0.265	0.250	0.035	0.197	0.367	0.349	0.039
		0.5	0.105	0.264	0.250	0.035	0.105	0.269	0.253	0.037	0.148	0.368	0.349	0.047
		0.7	0.125	0.265	0.228	0.042	0.125	0.267	0.227	0.043	0.175	0.371	0.321	0.058
		0.9	0.127	0.268	0.230	0.037	0.123	0.270	0.227	0.039	0.186	0.380	0.330	0.052

Table A.3
Case study 1: superimposition results for the RCGA-SBX algorithm.

β_1, β_2	Pop size	η	Fitness				MSE				MAX			
			m	M	μ	σ	m	M	μ	σ	m	M	μ	σ
1, 0	100	1.0	0.017	0.059	0.029	0.010	0.017	0.059	0.029	0.010	0.028	0.129	0.063	0.026
		2.0	0.018	0.072	0.039	0.014	0.018	0.072	0.039	0.014	0.037	0.173	0.088	0.038
		5.0	0.021	0.093	0.049	0.020	0.021	0.093	0.049	0.020	0.039	0.218	0.110	0.048
		10.0	0.028	0.233	0.096	0.063	0.028	0.233	0.096	0.063	0.067	0.390	0.188	0.097
		20.0	0.037	0.265	0.188	0.084	0.037	0.265	0.188	0.084	0.090	0.442	0.326	0.122
	500	1.0	0.017	0.023	0.019	0.002	0.017	0.023	0.019	0.002	0.028	0.057	0.051	0.006
		2.0	0.017	0.037	0.020	0.004	0.017	0.037	0.020	0.004	0.031	0.068	0.050	0.009
		5.0	0.017	0.197	0.038	0.032	0.017	0.197	0.038	0.032	0.032	0.541	0.085	0.094
		10.0	0.017	0.061	0.036	0.011	0.017	0.061	0.036	0.011	0.035	0.160	0.085	0.038
		20.0	0.019	0.157	0.057	0.035	0.019	0.157	0.057	0.035	0.039	0.293	0.127	0.068
0, 1	100	1.0	0.025	0.092	0.056	0.019	0.022	0.078	0.048	0.016	0.025	0.092	0.056	0.019
		2.0	0.032	0.184	0.066	0.033	0.028	0.154	0.056	0.026	0.032	0.184	0.066	0.033
		5.0	0.049	0.310	0.109	0.076	0.042	0.229	0.089	0.055	0.049	0.310	0.109	0.076
		10.0	0.052	0.389	0.237	0.121	0.045	0.283	0.177	0.085	0.052	0.389	0.237	0.121
		20.0	0.240	0.392	0.343	0.044	0.183	0.288	0.251	0.029	0.240	0.392	0.343	0.044
	500	1.0	0.022	0.058	0.029	0.008	0.021	0.055	0.027	0.007	0.022	0.058	0.029	0.008
		2.0	0.022	0.094	0.036	0.014	0.019	0.077	0.032	0.011	0.022	0.094	0.036	0.014
		5.0	0.024	0.078	0.046	0.014	0.023	0.069	0.040	0.013	0.024	0.078	0.046	0.014
		10.0	0.036	0.188	0.062	0.030	0.031	0.138	0.053	0.023	0.036	0.188	0.062	0.030
		20.0	0.027	0.376	0.176	0.124	0.025	0.274	0.132	0.088	0.027	0.376	0.176	0.124
0.5,0.5	100	1.0	0.019	0.072	0.033	0.011	0.020	0.073	0.034	0.011	0.025	0.099	0.044	0.017
		2.0	0.022	0.093	0.048	0.017	0.021	0.098	0.050	0.018	0.031	0.124	0.065	0.024
		5.0	0.024	0.275	0.076	0.058	0.027	0.277	0.076	0.059	0.031	0.385	0.107	0.081
		10.0	0.024	0.263	0.120	0.078	0.025	0.266	0.119	0.078	0.032	0.366	0.172	0.110
		20.0	0.024	0.267	0.204	0.084	0.023	0.270	0.205	0.087	0.034	0.378	0.287	0.115
	500	1.0	0.017	0.030	0.020	0.003	0.018	0.032	0.021	0.004	0.023	0.039	0.026	0.004
		2.0	0.017	0.053	0.024	0.008	0.018	0.060	0.026	0.009	0.023	0.064	0.031	0.009
		5.0	0.017	0.082	0.034	0.013	0.018	0.090	0.036	0.014	0.023	0.104	0.045	0.016
		10.0	0.018	0.093	0.040	0.018	0.020	0.085	0.041	0.016	0.023	0.141	0.055	0.028
		20.0	0.020	0.239	0.057	0.043	0.021	0.238	0.055	0.041	0.026	0.337	0.083	0.065

Table A.4
Case study 1: superimposition results for the CMA-ES algorithm.

β_1, β_2	Evaluations	θ	Fitness				MSE				MAX			
			m	M	μ	σ	m	M	μ	σ	m	M	μ	σ
1, 0	55,200	0.00001	0.017	0.151	0.058	0.045	0.017	0.151	0.058	0.045	0.043	0.238	0.109	0.062
		0.00010	0.017	0.175	0.044	0.036	0.017	0.175	0.044	0.036	0.039	0.239	0.089	0.051
		0.00100	0.017	0.175	0.051	0.046	0.017	0.175	0.051	0.046	0.038	0.494	0.115	0.099
		0.01000	0.017	0.168	0.057	0.046	0.017	0.168	0.057	0.046	0.051	0.276	0.108	0.067
		0.10000	0.017	0.117	0.050	0.035	0.017	0.117	0.050	0.035	0.049	0.215	0.093	0.052
		0.30000	0.017	0.906	0.157	0.220	0.017	0.906	0.157	0.220	0.046	1.258	0.269	0.334
	276,000	0.00001	0.017	0.031	0.018	0.003	0.017	0.031	0.018	0.003	0.045	0.052	0.051	0.001
		0.00010	0.017	0.043	0.021	0.009	0.017	0.043	0.021	0.009	0.039	0.137	0.061	0.028
		0.00100	0.017	0.044	0.019	0.008	0.017	0.044	0.019	0.008	0.051	0.142	0.060	0.027
		0.01000	0.017	0.043	0.018	0.005	0.017	0.043	0.018	0.005	0.031	0.134	0.053	0.016
		0.10000	0.017	0.018	0.017	0.000	0.017	0.018	0.017	0.000	0.050	0.055	0.051	0.001
		0.30000	0.017	0.096	0.024	0.020	0.017	0.096	0.024	0.020	0.049	0.190	0.064	0.035
0, 1	55,200	0.00001	0.022	0.355	0.109	0.072	0.019	0.251	0.076	0.050	0.022	0.355	0.109	0.072
		0.00010	0.022	0.340	0.118	0.076	0.020	0.243	0.085	0.053	0.022	0.340	0.118	0.076
		0.00100	0.022	0.304	0.102	0.073	0.020	0.154	0.072	0.045	0.022	0.304	0.102	0.073
		0.01000	0.022	0.283	0.120	0.082	0.019	0.191	0.083	0.055	0.022	0.283	0.120	0.082
		0.10000	0.022	0.296	0.088	0.069	0.019	0.186	0.065	0.047	0.022	0.296	0.088	0.069
		0.30000	0.022	1.258	0.248	0.331	0.020	0.906	0.168	0.224	0.022	1.258	0.248	0.331
	276,000	0.00001	0.022	0.087	0.028	0.017	0.020	0.067	0.025	0.012	0.022	0.087	0.028	0.017
		0.00010	0.022	0.090	0.029	0.020	0.021	0.076	0.026	0.016	0.022	0.090	0.029	0.020
		0.00100	0.022	0.088	0.029	0.020	0.020	0.064	0.025	0.012	0.022	0.088	0.029	0.020
		0.01000	0.022	0.089	0.026	0.017	0.020	0.069	0.023	0.011	0.022	0.089	0.026	0.017
		0.10000	0.022	0.034	0.025	0.004	0.020	0.031	0.023	0.003	0.022	0.034	0.025	0.004
		0.30000	0.023	0.194	0.057	0.051	0.021	0.129	0.044	0.032	0.023	0.194	0.057	0.051
0.5, 0.5	55,200	0.00001	0.017	0.492	0.075	0.090	0.018	0.483	0.071	0.088	0.023	0.693	0.110	0.128
		0.00010	0.017	0.235	0.077	0.051	0.018	0.222	0.071	0.048	0.023	0.344	0.115	0.078
		0.00100	0.017	0.149	0.072	0.043	0.018	0.131	0.068	0.041	0.023	0.233	0.104	0.064
		0.01000	0.017	0.163	0.074	0.044	0.018	0.154	0.068	0.041	0.023	0.238	0.111	0.066
		0.10000	0.017	0.191	0.055	0.049	0.018	0.159	0.051	0.042	0.023	0.309	0.081	0.079
		0.30000	0.017	0.908	0.182	0.224	0.018	0.906	0.167	0.212	0.023	1.258	0.271	0.327
	276,000	0.00001	0.017	0.059	0.027	0.018	0.018	0.052	0.026	0.014	0.023	0.092	0.039	0.030
		0.00010	0.017	0.059	0.019	0.008	0.018	0.052	0.019	0.006	0.023	0.092	0.026	0.013
		0.00100	0.017	0.059	0.020	0.011	0.018	0.052	0.020	0.008	0.023	0.092	0.028	0.017
		0.01000	0.017	0.059	0.023	0.013	0.018	0.052	0.022	0.011	0.023	0.093	0.032	0.022
		0.10000	0.017	0.020	0.018	0.001	0.018	0.021	0.019	0.001	0.023	0.027	0.024	0.001
		0.30000	0.017	0.086	0.025	0.015	0.018	0.084	0.025	0.015	0.023	0.122	0.033	0.022

Table A.5
Case study 2: superimposition results for the BCGA algorithm.

β_1, β_2	Pop size	Fitness				MSE				MAX			
		m	M	μ	σ	m	M	μ	σ	m	M	μ	σ
1, 0	100	0.021	0.268	0.092	0.080	0.021	0.268	0.092	0.080	0.046	0.392	0.160	0.099
	500	0.009	0.190	0.029	0.036	0.009	0.190	0.029	0.036	0.019	0.258	0.059	0.051
0, 1	100	0.041	0.373	0.293	0.097	0.036	0.289	0.236	0.077	0.041	0.373	0.293	0.097
	500	0.017	0.344	0.102	0.100	0.013	0.275	0.083	0.081	0.017	0.344	0.102	0.100
0.5, 0.5	100	0.027	0.271	0.176	0.081	0.028	0.284	0.181	0.088	0.036	0.360	0.237	0.103
	500	0.011	0.114	0.039	0.027	0.011	0.122	0.039	0.027	0.013	0.147	0.055	0.038

Table A.6
Case study 2: superimposition results for the RCGA-BLX-α algorithm.

β_1, β_2	Pop size	α	Fitness				MSE				*MAX*			
			m	M	μ	σ	m	M	μ	σ	m	M	μ	σ
1, 0	100	0.1	0.023	0.133	0.072	0.021	0.023	0.133	0.072	0.021	0.051	0.273	0.168	0.058
		0.3	0.008	0.089	0.038	0.024	0.008	0.089	0.038	0.024	0.027	0.224	0.092	0.054
		0.5	0.007	0.016	0.010	0.003	0.007	0.016	0.010	0.003	0.020	0.048	0.030	0.007
		0.7	0.011	0.028	0.018	0.004	0.011	0.028	0.018	0.004	0.018	0.064	0.039	0.013
		0.9	0.029	0.111	0.052	0.017	0.029	0.111	0.052	0.017	0.050	0.212	0.104	0.041
	500	0.1	0.034	0.090	0.065	0.014	0.034	0.090	0.065	0.014	0.074	0.235	0.143	0.038
		0.3	0.008	0.058	0.019	0.012	0.008	0.058	0.019	0.012	0.028	0.147	0.050	0.028
		0.5	0.007	0.011	0.008	0.001	0.007	0.011	0.008	0.001	0.023	0.029	0.029	0.001
		0.7	0.015	0.028	0.021	0.003	0.015	0.028	0.021	0.003	0.021	0.069	0.040	0.011
		0.9	0.013	0.147	0.085	0.028	0.013	0.147	0.085	0.028	0.032	0.350	0.163	0.069

(*continued on next page*)

Table A.6 (*continued*)

β_1, β_2	Pop size	α	Fitness				MSE				*MAX*			
			m	M	μ	σ	m	M	μ	σ	m	M	μ	σ
0, 1	100	0.1	0.170	0.348	0.320	0.045	0.135	0.288	0.264	0.038	0.170	0.348	0.320	0.045
		0.3	0.061	0.343	0.231	0.100	0.054	0.284	0.187	0.084	0.061	0.343	0.231	0.100
		0.5	0.013	0.076	0.033	0.021	0.012	0.068	0.028	0.018	0.013	0.076	0.033	0.021
		0.7	0.019	0.043	0.030	0.006	0.013	0.031	0.021	0.005	0.019	0.043	0.030	0.006
		0.9	0.053	0.249	0.166	0.049	0.026	0.191	0.119	0.037	0.053	0.249	0.166	0.049
	500	0.1	0.167	0.346	0.316	0.041	0.129	0.287	0.261	0.036	0.167	0.346	0.316	0.041
		0.3	0.067	0.345	0.210	0.093	0.057	0.286	0.169	0.083	0.067	0.345	0.210	0.093
		0.5	0.013	0.053	0.019	0.007	0.012	0.045	0.015	0.006	0.013	0.053	0.019	0.007
		0.7	0.022	0.056	0.038	0.006	0.015	0.037	0.027	0.006	0.022	0.056	0.038	0.006
		0.9	0.112	0.274	0.217	0.044	0.057	0.217	0.152	0.033	0.112	0.274	0.217	0.044
0.5, 0.5	100	0.1	0.043	0.190	0.123	0.034	0.047	0.202	0.120	0.038	0.056	0.259	0.178	0.047
		0.3	0.012	0.152	0.073	0.036	0.012	0.153	0.071	0.037	0.016	0.223	0.104	0.051
		0.5	0.010	0.022	0.014	0.003	0.010	0.020	0.014	0.003	0.014	0.033	0.020	0.005
		0.7	0.013	0.032	0.021	0.005	0.013	0.031	0.020	0.005	0.019	0.046	0.031	0.007
		0.9	0.028	0.161	0.074	0.033	0.025	0.155	0.069	0.031	0.043	0.258	0.111	0.052
	500	0.1	0.066	0.110	0.089	0.013	0.062	0.108	0.081	0.011	0.099	0.183	0.136	0.023
		0.3	0.011	0.082	0.049	0.017	0.010	0.089	0.049	0.018	0.016	0.110	0.067	0.023
		0.5	0.010	0.014	0.012	0.001	0.010	0.014	0.011	0.001	0.014	0.019	0.017	0.001
		0.7	0.016	0.032	0.024	0.003	0.016	0.028	0.023	0.003	0.023	0.054	0.036	0.006
		0.9	0.086	0.161	0.123	0.022	0.083	0.169	0.118	0.023	0.116	0.231	0.179	0.032

Table A.7
Case study 2: superimposition results for the RCGA-SBX algorithm.

β_1, β_2	Pop size	η	Fitness				MSE				MAX			
			m	M	μ	σ	m	M	μ	σ	m	M	μ	σ
1, 0	100	1.0	0.008	0.062	0.024	0.017	0.008	0.062	0.024	0.017	0.016	0.197	0.062	0.050
		2.0	0.008	0.089	0.032	0.024	0.008	0.089	0.032	0.024	0.020	0.322	0.091	0.072
		5.0	0.010	0.135	0.056	0.034	0.010	0.135	0.056	0.034	0.026	0.493	0.167	0.117
		10.0	0.010	0.133	0.071	0.035	0.010	0.133	0.071	0.035	0.027	0.396	0.179	0.099
		20.0	0.011	0.105	0.066	0.028	0.011	0.105	0.066	0.028	0.021	0.343	0.159	0.073
	500	1.0	0.007	0.014	0.008	0.001	0.007	0.014	0.008	0.001	0.017	0.040	0.026	0.004
		2.0	0.007	0.013	0.009	0.002	0.007	0.013	0.009	0.002	0.018	0.033	0.026	0.004
		5.0	0.008	0.052	0.013	0.010	0.008	0.052	0.013	0.010	0.016	0.174	0.036	0.029
		10.0	0.008	0.076	0.019	0.015	0.008	0.076	0.019	0.015	0.015	0.162	0.045	0.032
		20.0	0.008	0.105	0.029	0.023	0.008	0.105	0.029	0.023	0.019	0.260	0.071	0.056
0, 1	100	1.0	0.012	0.131	0.042	0.028	0.012	0.094	0.035	0.022	0.012	0.131	0.042	0.028
		2.0	0.013	0.263	0.074	0.057	0.011	0.229	0.060	0.049	0.013	0.263	0.074	0.057
		5.0	0.027	0.318	0.123	0.077	0.023	0.281	0.101	0.066	0.027	0.318	0.123	0.077
		10.0	0.021	0.360	0.190	0.089	0.017	0.289	0.154	0.075	0.021	0.360	0.190	0.089
		20.0	0.051	0.359	0.223	0.104	0.045	0.289	0.180	0.085	0.051	0.359	0.223	0.104
	500	1.0	0.012	0.028	0.014	0.003	0.012	0.025	0.013	0.002	0.012	0.028	0.014	0.003
		2.0	0.012	0.035	0.019	0.007	0.011	0.030	0.016	0.006	0.012	0.035	0.019	0.007
		5.0	0.013	0.113	0.045	0.032	0.012	0.099	0.038	0.025	0.013	0.113	0.045	0.032
		10.0	0.013	0.164	0.063	0.048	0.012	0.125	0.052	0.038	0.013	0.164	0.063	0.048
		20.0	0.013	0.209	0.089	0.054	0.013	0.164	0.072	0.043	0.013	0.209	0.089	0.054
0.5, 0.5	100	1.0	0.010	0.075	0.022	0.015	0.010	0.070	0.022	0.015	0.012	0.110	0.031	0.022
		2.0	0.011	0.093	0.039	0.023	0.011	0.105	0.039	0.022	0.014	0.142	0.056	0.034
		5.0	0.012	0.135	0.049	0.031	0.012	0.143	0.049	0.031	0.016	0.206	0.069	0.044
		10.0	0.012	0.223	0.082	0.050	0.012	0.227	0.078	0.047	0.016	0.336	0.120	0.075
		20.0	0.021	0.270	0.125	0.083	0.020	0.286	0.122	0.088	0.029	0.364	0.178	0.112
	500	1.0	0.009	0.013	0.010	0.001	0.009	0.013	0.010	0.001	0.013	0.018	0.014	0.001
		2.0	0.010	0.015	0.011	0.001	0.009	0.014	0.011	0.001	0.013	0.022	0.015	0.002
		5.0	0.010	0.066	0.020	0.016	0.010	0.073	0.021	0.017	0.014	0.083	0.028	0.020
		10.0	0.010	0.118	0.032	0.026	0.010	0.096	0.031	0.022	0.013	0.200	0.045	0.043
		20.0	0.010	0.144	0.047	0.036	0.010	0.123	0.046	0.035	0.014	0.229	0.064	0.052

Table A.8
Case study 2: superimposition results for the CMA-ES algorithm.

β_1, β_2	Evaluations	θ	Fitness				MSE				*MAX*			
			m	M	μ	σ	m	M	μ	σ	m	M	μ	σ
1, 0	55,200	0.00001	0.007	0.265	0.080	0.084	0.007	0.265	0.080	0.084	0.025	0.394	0.147	0.129
		0.00010	0.007	0.273	0.095	0.105	0.007	0.273	0.095	0.105	0.023	0.413	0.156	0.150
		0.00100	0.007	0.275	0.097	0.088	0.007	0.275	0.097	0.088	0.022	0.482	0.174	0.142
		0.01000	0.007	0.276	0.111	0.109	0.007	0.276	0.111	0.109	0.020	0.516	0.182	0.161
		0.10000	0.007	0.269	0.173	0.101	0.007	0.269	0.173	0.101	0.026	0.434	0.267	0.142
		0.30000	0.007	0.712	0.277	0.135	0.007	0.712	0.277	0.135	0.026	0.870	0.416	0.183
	276,000	0.00001	0.007	0.091	0.010	0.015	0.007	0.091	0.010	0.015	0.019	0.233	0.031	0.038
		0.00010	0.007	0.008	0.008	0.000	0.007	0.008	0.008	0.000	0.019	0.027	0.024	0.003
		0.00100	0.007	0.030	0.008	0.004	0.007	0.030	0.008	0.004	0.019	0.128	0.028	0.019
		0.01000	0.007	0.101	0.014	0.023	0.007	0.101	0.014	0.023	0.016	0.257	0.040	0.059
		0.10000	0.007	0.146	0.025	0.035	0.007	0.146	0.025	0.035	0.020	0.284	0.055	0.061
		0.30000	0.007	0.261	0.121	0.106	0.007	0.261	0.121	0.106	0.019	0.422	0.194	0.154
0, 1	55,200	0.00001	0.012	0.353	0.153	0.116	0.012	0.277	0.116	0.089	0.012	0.353	0.153	0.116
		0.00010	0.012	0.360	0.124	0.112	0.012	0.284	0.091	0.084	0.012	0.360	0.124	0.112
		0.00100	0.012	0.359	0.158	0.128	0.012	0.284	0.122	0.101	0.012	0.359	0.158	0.128
		0.01000	0.012	0.361	0.152	0.111	0.012	0.283	0.111	0.085	0.012	0.361	0.152	0.111
		0.10000	0.012	0.362	0.304	0.095	0.012	0.288	0.234	0.077	0.012	0.362	0.304	0.095
		0.30000	0.012	0.870	0.415	0.185	0.012	0.712	0.299	0.131	0.012	0.870	0.415	0.185
	276,000	0.00001	0.012	0.166	0.020	0.030	0.011	0.122	0.017	0.021	0.012	0.166	0.020	0.030
		0.00010	0.012	0.012	0.012	0.000	0.011	0.012	0.012	0.000	0.012	0.012	0.012	0.000
		0.00100	0.012	0.030	0.013	0.003	0.012	0.024	0.012	0.002	0.012	0.030	0.013	0.003
		0.01000	0.012	0.012	0.012	0.000	0.012	0.012	0.012	0.000	0.012	0.012	0.012	0.000
		0.10000	0.012	0.324	0.118	0.100	0.012	0.245	0.083	0.074	0.012	0.324	0.118	0.100
		0.30000	0.012	0.358	0.273	0.097	0.012	0.280	0.197	0.079	0.012	0.358	0.273	0.097
0.5, 0.5	55,200	0.00001	0.010	0.261	0.096	0.090	0.009	0.261	0.092	0.089	0.014	0.354	0.135	0.123
		0.00010	0.010	0.269	0.106	0.092	0.009	0.276	0.103	0.092	0.014	0.355	0.148	0.125
		0.00100	0.010	0.272	0.109	0.086	0.009	0.282	0.104	0.085	0.013	0.355	0.155	0.119
		0.01000	0.010	0.268	0.139	0.102	0.009	0.278	0.137	0.102	0.014	0.365	0.191	0.138
		0.10000	0.049	0.278	0.243	0.048	0.047	0.287	0.238	0.055	0.069	0.402	0.335	0.060
		0.30000	0.053	0.676	0.285	0.133	0.037	0.712	0.280	0.133	0.093	0.870	0.393	0.185
	276,000	0.00001	0.010	0.117	0.017	0.027	0.009	0.110	0.016	0.025	0.014	0.170	0.024	0.040
		0.00010	0.010	0.010	0.010	0.000	0.009	0.010	0.009	0.000	0.014	0.014	0.014	0.000
		0.00100	0.010	0.010	0.010	0.000	0.009	0.010	0.009	0.000	0.013	0.014	0.014	0.000
		0.01000	0.010	0.086	0.012	0.014	0.009	0.088	0.012	0.014	0.014	0.113	0.017	0.018
		0.10000	0.010	0.250	0.082	0.082	0.009	0.254	0.078	0.078	0.014	0.333	0.117	0.117
		0.30000	0.010	0.284	0.146	0.102	0.010	0.293	0.142	0.102	0.014	0.389	0.203	0.139

Table A.9
Case study 3, pose 1: superimposition results for the BCGA algorithm.

β_1, β_2	Pop size	Fitness				MSE				MAX			
		m	M	μ	σ	m	M	μ	σ	m	M	μ	σ
1, 0	100	0.085	0.137	0.122	0.013	0.085	0.137	0.122	0.013	0.229	0.361	0.324	0.034
	500	0.030	0.129	0.101	0.025	0.030	0.129	0.101	0.025	0.062	0.344	0.271	0.065
0, 1	100	0.036	0.244	0.213	0.040	0.029	0.171	0.151	0.028	0.036	0.244	0.213	0.040
	500	0.061	0.229	0.189	0.036	0.051	0.161	0.133	0.024	0.061	0.229	0.189	0.036
0.5, 0.5	100	0.038	0.175	0.159	0.025	0.037	0.168	0.153	0.024	0.050	0.240	0.216	0.034
	500	0.035	0.159	0.125	0.034	0.035	0.152	0.118	0.034	0.045	0.217	0.174	0.045

Table A.10
Case study 3, pose 1: superimposition results for the RCGA-BLX-α algorithm.

β_1, β_2	Pop size	α	Fitness				MSE				MAX			
			m	M	μ	σ	m	M	μ	σ	m	M	μ	σ
1, 0	500	0.1	0.106	0.125	0.120	0.004	0.106	0.125	0.120	0.004	0.288	0.336	0.323	0.010
		0.3	0.079	0.122	0.112	0.011	0.079	0.122	0.112	0.011	0.158	0.330	0.300	0.041
		0.5	0.027	0.079	0.054	0.011	0.027	0.079	0.054	0.011	0.051	0.225	0.144	0.039
		0.7	0.040	0.110	0.076	0.019	0.040	0.110	0.076	0.019	0.100	0.297	0.195	0.061
		0.9	0.071	0.119	0.102	0.012	0.071	0.119	0.102	0.012	0.113	0.308	0.251	0.051
	1000	0.1	0.075	0.124	0.118	0.010	0.075	0.124	0.118	0.010	0.192	0.335	0.315	0.030
		0.3	0.040	0.121	0.103	0.023	0.040	0.121	0.103	0.023	0.113	0.328	0.272	0.072
		0.5	0.038	0.086	0.063	0.012	0.038	0.086	0.063	0.012	0.069	0.240	0.164	0.044
		0.7	0.038	0.112	0.074	0.016	0.038	0.112	0.074	0.016	0.094	0.307	0.191	0.053
		0.9	0.067	0.118	0.102	0.014	0.067	0.118	0.102	0.014	0.138	0.321	0.257	0.049

(*continued on next page*)

Table A.10 (*continued*)

β_1, β_2	Pop size	α	Fitness				MSE				MAX			
			m	M	μ	σ	m	M	μ	σ	m	M	μ	σ
0, 1	500	0.1	0.191	0.223	0.214	0.005	0.129	0.162	0.156	0.006	0.191	0.223	0.214	0.005
		0.3	0.195	0.223	0.215	0.006	0.139	0.159	0.154	0.004	0.195	0.223	0.215	0.006
		0.5	0.135	0.225	0.205	0.026	0.093	0.159	0.144	0.018	0.135	0.225	0.205	0.026
		0.7	0.133	0.228	0.208	0.023	0.095	0.168	0.146	0.017	0.133	0.228	0.208	0.023
		0.9	0.082	0.217	0.186	0.033	0.046	0.153	0.128	0.028	0.082	0.217	0.186	0.033
	1000	0.1	0.169	0.219	0.212	0.011	0.117	0.165	0.155	0.010	0.169	0.219	0.212	0.011
		0.3	0.058	0.223	0.203	0.034	0.036	0.160	0.146	0.024	0.058	0.223	0.203	0.034
		0.5	0.080	0.224	0.188	0.042	0.052	0.160	0.130	0.033	0.080	0.224	0.188	0.042
		0.7	0.129	0.227	0.197	0.027	0.095	0.161	0.139	0.019	0.129	0.227	0.197	0.027
		0.9	0.100	0.217	0.180	0.030	0.071	0.154	0.124	0.023	0.100	0.217	0.180	0.030
0.5, 0.5	500	0.1	0.142	0.166	0.160	0.006	0.129	0.155	0.149	0.006	0.190	0.224	0.215	0.007
		0.3	0.072	0.166	0.150	0.023	0.070	0.156	0.137	0.025	0.093	0.223	0.204	0.028
		0.5	0.036	0.164	0.127	0.037	0.036	0.153	0.113	0.038	0.046	0.239	0.177	0.049
		0.7	0.062	0.166	0.125	0.029	0.048	0.150	0.109	0.029	0.094	0.264	0.176	0.041
		0.9	0.070	0.157	0.124	0.027	0.052	0.146	0.110	0.027	0.092	0.231	0.175	0.038
	1000	0.1	0.091	0.164	0.154	0.018	0.081	0.153	0.143	0.019	0.128	0.220	0.207	0.023
		0.3	0.050	0.166	0.134	0.035	0.047	0.155	0.121	0.037	0.065	0.222	0.184	0.044
		0.5	0.069	0.161	0.119	0.032	0.055	0.150	0.103	0.032	0.095	0.232	0.167	0.044
		0.7	0.064	0.159	0.130	0.023	0.045	0.147	0.113	0.025	0.104	0.246	0.182	0.031
		0.9	0.065	0.149	0.118	0.023	0.059	0.136	0.100	0.023	0.088	0.242	0.168	0.038

Table A.11
Case study 3, pose 1: superimposition results for the RCGA-SBX algorithm.

β_1, β_2	Pop size	η	Fitness				MSE				MAX			
			m	M	μ	σ	m	M	μ	σ	m	M	μ	σ
1, 0	100	1.0	0.015	0.044	0.029	0.010	0.015	0.044	0.029	0.010	0.036	0.110	0.065	0.023
		2.0	0.015	0.047	0.029	0.012	0.015	0.047	0.029	0.012	0.034	0.147	0.065	0.028
		5.0	0.015	0.048	0.033	0.009	0.015	0.048	0.033	0.009	0.036	0.181	0.080	0.032
		10.0	0.022	0.089	0.038	0.014	0.022	0.089	0.038	0.014	0.037	0.244	0.092	0.047
		20.0	0.025	0.126	0.082	0.028	0.025	0.126	0.082	0.028	0.038	0.333	0.225	0.077
	500	1.0	0.015	0.033	0.017	0.005	0.015	0.033	0.017	0.005	0.034	0.087	0.044	0.015
		2.0	0.015	0.033	0.017	0.005	0.015	0.033	0.017	0.005	0.034	0.092	0.048	0.018
		5.0	0.015	0.038	0.022	0.008	0.015	0.038	0.022	0.008	0.034	0.196	0.054	0.033
		10.0	0.015	0.040	0.023	0.007	0.015	0.040	0.023	0.007	0.034	0.105	0.058	0.023
		20.0	0.015	0.040	0.026	0.008	0.015	0.040	0.026	0.008	0.034	0.113	0.066	0.026
0, 1	100	1.0	0.029	0.060	0.047	0.010	0.021	0.048	0.037	0.008	0.029	0.060	0.047	0.010
		2.0	0.032	0.069	0.048	0.010	0.021	0.053	0.039	0.008	0.032	0.069	0.048	0.010
		5.0	0.034	0.217	0.079	0.057	0.022	0.156	0.059	0.040	0.034	0.217	0.079	0.057
		10.0	0.034	0.232	0.118	0.068	0.022	0.163	0.086	0.048	0.034	0.232	0.118	0.068
		20.0	0.038	0.240	0.172	0.054	0.032	0.173	0.123	0.038	0.038	0.240	0.172	0.054
	500	1.0	0.028	0.045	0.033	0.006	0.022	0.041	0.028	0.008	0.028	0.045	0.033	0.006
		2.0	0.028	0.051	0.034	0.008	0.021	0.046	0.027	0.007	0.028	0.051	0.034	0.008
		5.0	0.029	0.067	0.041	0.011	0.021	0.057	0.034	0.010	0.029	0.067	0.041	0.011
		10.0	0.028	0.199	0.052	0.031	0.021	0.152	0.041	0.024	0.028	0.199	0.052	0.031
		20.0	0.029	0.210	0.080	0.055	0.021	0.155	0.061	0.040	0.029	0.210	0.080	0.055
0.5, 0.5	100	1.0	0.021	0.058	0.038	0.009	0.017	0.058	0.037	0.009	0.031	0.073	0.048	0.011
		2.0	0.021	0.072	0.041	0.012	0.017	0.063	0.040	0.010	0.030	0.107	0.053	0.017
		5.0	0.022	0.053	0.040	0.008	0.020	0.052	0.039	0.008	0.030	0.074	0.052	0.012
		10.0	0.027	0.169	0.065	0.045	0.022	0.158	0.061	0.042	0.039	0.225	0.088	0.061
		20.0	0.028	0.171	0.111	0.048	0.025	0.161	0.102	0.045	0.038	0.227	0.150	0.064
	500	1.0	0.021	0.035	0.022	0.003	0.016	0.038	0.018	0.005	0.029	0.040	0.032	0.002
		2.0	0.021	0.040	0.024	0.005	0.016	0.041	0.020	0.007	0.029	0.048	0.034	0.005
		5.0	0.021	0.042	0.028	0.007	0.016	0.042	0.027	0.009	0.029	0.053	0.037	0.007
		10.0	0.021	0.051	0.029	0.007	0.018	0.050	0.027	0.008	0.029	0.065	0.037	0.008
		20.0	0.023	0.081	0.043	0.016	0.021	0.067	0.040	0.012	0.030	0.125	0.058	0.026

Table A.12
Case study 3, pose 1: superimposition results for the CMA-ES algorithm.

β_1, β_2	Evaluations	θ	Fitness				MSE				MAX			
			m	M	μ	σ	m	M	μ	σ	m	M	μ	σ
1, 0	55,200	0.00001	0.015	0.077	0.034	0.021	0.015	0.077	0.034	0.021	0.040	0.174	0.077	0.044
		0.00010	0.015	0.064	0.026	0.016	0.015	0.064	0.026	0.016	0.040	0.183	0.065	0.042
		0.00100	0.015	0.067	0.027	0.017	0.015	0.067	0.027	0.017	0.040	0.177	0.065	0.037
		0.01000	0.015	0.064	0.028	0.019	0.015	0.064	0.028	0.019	0.040	0.156	0.062	0.034
		0.10000	0.015	0.104	0.035	0.024	0.015	0.104	0.035	0.024	0.038	0.273	0.083	0.058
		0.30000	0.015	1.018	0.140	0.207	0.015	1.018	0.140	0.207	0.040	1.141	0.226	0.246
	276,000	0.00001	0.015	0.042	0.018	0.009	0.015	0.042	0.018	0.009	0.040	0.086	0.046	0.014
		0.00010	0.015	0.032	0.015	0.003	0.015	0.032	0.015	0.003	0.039	0.085	0.042	0.008
		0.00100	0.015	0.015	0.015	0.000	0.015	0.015	0.015	0.000	0.040	0.041	0.040	0.000
		0.01000	0.015	0.043	0.017	0.007	0.015	0.043	0.017	0.007	0.040	0.087	0.043	0.011
		0.10000	0.015	0.034	0.016	0.003	0.015	0.034	0.016	0.003	0.040	0.085	0.042	0.008
		0.30000	0.015	0.076	0.036	0.024	0.015	0.076	0.036	0.024	0.040	0.209	0.084	0.052
0, 1	55,200	0.00001	0.028	0.137	0.059	0.038	0.021	0.092	0.043	0.024	0.028	0.137	0.059	0.038
		0.00010	0.028	0.118	0.055	0.030	0.022	0.070	0.039	0.016	0.028	0.118	0.055	0.030
		0.00100	0.028	0.119	0.055	0.032	0.022	0.072	0.038	0.017	0.028	0.119	0.055	0.032
		0.01000	0.028	0.254	0.071	0.047	0.022	0.175	0.050	0.030	0.028	0.254	0.071	0.047
		0.10000	0.028	0.146	0.087	0.037	0.023	0.104	0.058	0.024	0.028	0.146	0.087	0.037
		0.30000	0.028	1.141	0.209	0.237	0.024	1.018	0.147	0.198	0.028	1.141	0.209	0.237
	276,000	0.00001	0.028	0.060	0.032	0.010	0.022	0.046	0.026	0.008	0.028	0.060	0.032	0.010
		0.00010	0.028	0.059	0.034	0.012	0.022	0.045	0.027	0.008	0.028	0.059	0.034	0.012
		0.00100	0.028	0.060	0.034	0.010	0.022	0.046	0.029	0.009	0.028	0.060	0.034	0.010
		0.01000	0.028	0.061	0.034	0.010	0.022	0.046	0.028	0.008	0.028	0.061	0.034	0.010
		0.10000	0.028	0.074	0.031	0.009	0.022	0.053	0.025	0.007	0.028	0.074	0.031	0.009
		0.30000	0.028	0.137	0.070	0.037	0.022	0.089	0.047	0.022	0.028	0.137	0.070	0.037
0.5, 0.5	55,200	0.00001	0.021	0.085	0.041	0.023	0.016	0.078	0.035	0.020	0.031	0.140	0.058	0.034
		0.00010	0.021	0.082	0.051	0.022	0.016	0.079	0.045	0.019	0.031	0.123	0.071	0.032
		0.00100	0.021	0.084	0.048	0.023	0.016	0.079	0.042	0.029	0.031	0.126	0.066	0.033
		0.01000	0.021	0.086	0.045	0.024	0.016	0.079	0.039	0.021	0.031	0.133	0.062	0.034
		0.10000	0.021	0.093	0.048	0.027	0.016	0.087	0.040	0.024	0.031	0.135	0.069	0.039
		0.30000	0.021	0.970	0.141	0.201	0.016	1.018	0.131	0.204	0.031	1.141	0.187	0.245
	276,000	0.00001	0.021	0.047	0.024	0.008	0.016	0.046	0.020	0.009	0.031	0.060	0.034	0.008
		0.00010	0.021	0.038	0.023	0.005	0.016	0.040	0.019	0.008	0.031	0.044	0.033	0.003
		0.00100	0.021	0.046	0.023	0.007	0.016	0.044	0.020	0.009	0.031	0.058	0.034	0.007
		0.01000	0.021	0.048	0.024	0.008	0.016	0.046	0.020	0.009	0.031	0.061	0.034	0.009
		0.10000	0.021	0.061	0.022	0.007	0.016	0.054	0.018	0.007	0.031	0.084	0.033	0.010
		0.30000	0.021	0.110	0.052	0.031	0.016	0.091	0.043	0.025	0.031	0.170	0.076	0.046

Table A.13
Case study 3, pose 2: superimposition results for the BCGA algorithm.

β_1, β_2	Pop size	Fitness				MSE				MAX			
		m	M	μ	σ	m	M	μ	σ	m	M	μ	σ
1, 0	100	0.077	0.193	0.166	0.030	0.077	0.193	0.166	0.030	0.129	0.414	0.351	0.067
	500	0.043	0.180	0.123	0.041	0.043	0.180	0.123	0.041	0.120	0.374	0.259	0.077
0, 1	100	0.148	0.300	0.269	0.041	0.102	0.215	0.190	0.030	0.148	0.300	0.269	0.041
	500	0.094	0.283	0.201	0.071	0.066	0.198	0.141	0.051	0.094	0.283	0.201	0.071
0.5, 0.5	100	0.101	0.214	0.196	0.026	0.090	0.209	0.191	0.027	0.153	0.298	0.274	0.035
	500	0.066	0.190	0.128	0.039	0.052	0.183	0.122	0.039	0.092	0.262	0.179	0.053

Table A.14
Case study 3, pose 2: superimposition results for the RCGA-BLX-α algorithm.

β_1, β_2	Pop size	α	Fitness				MSE				*MAX*			
			m	M	μ	σ	m	M	μ	σ	m	M	μ	σ
1, 0	500	0.1	0.092	0.177	0.148	0.021	0.092	0.177	0.148	0.021	0.172	0.376	0.311	0.053
		0.3	0.055	0.158	0.078	0.025	0.055	0.158	0.078	0.025	0.104	0.364	0.165	0.059
		0.5	0.052	0.058	0.055	0.001	0.052	0.058	0.055	0.001	0.106	0.136	0.124	0.006
		0.7	0.046	0.094	0.058	0.010	0.046	0.094	0.058	0.010	0.111	0.216	0.143	0.028
		0.9	0.088	0.166	0.136	0.020	0.088	0.166	0.136	0.020	0.187	0.396	0.273	0.060
	1000	0.1	0.071	0.176	0.136	0.028	0.071	0.176	0.136	0.028	0.139	0.381	0.292	0.071
		0.3	0.051	0.114	0.072	0.017	0.051	0.114	0.072	0.017	0.107	0.249	0.146	0.037
		0.5	0.054	0.058	0.057	0.001	0.054	0.058	0.057	0.001	0.113	0.134	0.122	0.005
		0.7	0.047	0.074	0.058	0.007	0.047	0.074	0.058	0.007	0.104	0.190	0.134	0.021
		0.9	0.091	0.158	0.133	0.019	0.091	0.158	0.133	0.019	0.149	0.380	0.275	0.063

(*continued on next page*)

Table A.14 (*continued*)

β_1, β_2	Pop size	α	Fitness				MSE				*MAX*			
			m	*M*	μ	σ	*m*	*M*	μ	σ	*m*	*M*	μ	σ
0, 1	500	0.1	0.255	0.287	0.281	0.007	0.183	0.211	0.204	0.006	0.255	0.287	0.281	0.007
		0.3	0.111	0.287	0.271	0.035	0.057	0.211	0.193	0.029	0.111	0.287	0.271	0.035
		0.5	0.155	0.280	0.242	0.042	0.067	0.197	0.165	0.039	0.155	0.280	0.242	0.042
		0.7	0.119	0.285	0.228	0.036	0.079	0.201	0.156	0.029	0.119	0.285	0.228	0.036
		0.9	0.142	0.281	0.225	0.035	0.093	0.192	0.153	0.026	0.142	0.281	0.225	0.035
	1000	0.1	0.182	0.287	0.271	0.027	0.132	0.211	0.197	0.022	0.182	0.287	0.271	0.027
		0.3	0.182	0.284	0.258	0.034	0.104	0.207	0.180	0.030	0.182	0.284	0.258	0.034
		0.5	0.128	0.280	0.237	0.051	0.056	0.196	0.162	0.043	0.128	0.280	0.237	0.051
		0.7	0.170	0.281	0.236	0.034	0.112	0.202	0.161	0.025	0.170	0.281	0.236	0.034
		0.9	0.160	0.269	0.221	0.031	0.101	0.190	0.147	0.030	0.160	0.269	0.221	0.031
0.5, 0.5	500	0.1	0.179	0.202	0.197	0.006	0.174	0.197	0.191	0.006	0.249	0.283	0.274	0.008
		0.3	0.137	0.204	0.197	0.013	0.128	0.198	0.191	0.013	0.196	0.285	0.275	0.016
		0.5	0.062	0.197	0.106	0.042	0.043	0.191	0.094	0.045	0.106	0.274	0.160	0.052
		0.7	0.065	0.132	0.091	0.021	0.050	0.129	0.082	0.023	0.102	0.192	0.136	0.028
		0.9	0.092	0.189	0.148	0.025	0.073	0.185	0.131	0.027	0.128	0.299	0.225	0.040
	1000	0.1	0.134	0.203	0.192	0.014	0.132	0.197	0.186	0.013	0.182	0.282	0.268	0.020
		0.3	0.073	0.204	0.164	0.046	0.049	0.197	0.154	0.050	0.116	0.286	0.233	0.056
		0.5	0.069	0.188	0.115	0.033	0.055	0.182	0.105	0.035	0.109	0.261	0.169	0.042
		0.7	0.067	0.160	0.098	0.026	0.053	0.147	0.085	0.024	0.108	0.269	0.148	0.040
		0.9	0.072	0.189	0.145	0.025	0.059	0.181	0.132	0.024	0.115	0.281	0.213	0.039

Table A.15
Case study 3, pose 2: superimposition results for the RCGA-SBX algorithm.

β_1, β_2	Pop size	η	Fitness				MSE				MAX			
			m	*M*	μ	σ	*m*	*M*	μ	σ	*m*	*M*	μ	σ
1, 0	100	1.0	0.036	0.062	0.048	0.010	0.036	0.062	0.048	0.010	0.111	0.291	0.153	0.032
		2.0	0.036	0.096	0.052	0.015	0.036	0.096	0.052	0.015	0.120	0.230	0.156	0.028
		5.0	0.037	0.086	0.056	0.014	0.037	0.086	0.056	0.014	0.118	0.213	0.155	0.024
		10.0	0.039	0.142	0.063	0.022	0.039	0.142	0.063	0.022	0.119	0.313	0.158	0.040
		20.0	0.037	0.184	0.118	0.049	0.037	0.184	0.118	0.049	0.116	0.395	0.264	0.098
	500	1.0	0.036	0.038	0.036	0.000	0.036	0.038	0.036	0.000	0.131	0.145	0.143	0.002
		2.0	0.036	0.060	0.040	0.008	0.036	0.060	0.040	0.008	0.103	0.246	0.144	0.021
		5.0	0.036	0.067	0.043	0.008	0.036	0.067	0.043	0.008	0.116	0.198	0.143	0.014
		10.0	0.036	0.065	0.049	0.009	0.036	0.065	0.049	0.009	0.109	0.199	0.147	0.020
		20.0	0.036	0.102	0.053	0.013	0.036	0.102	0.053	0.013	0.100	0.202	0.135	0.022
0, 1	100	1.0	0.090	0.122	0.103	0.007	0.059	0.101	0.072	0.009	0.090	0.122	0.103	0.007
		2.0	0.091	0.212	0.109	0.023	0.060	0.144	0.075	0.016	0.091	0.212	0.109	0.023
		5.0	0.094	0.304	0.124	0.042	0.059	0.216	0.086	0.032	0.094	0.304	0.124	0.042
		10.0	0.104	0.298	0.196	0.074	0.066	0.213	0.138	0.055	0.104	0.298	0.196	0.074
		20.0	0.103	0.299	0.231	0.066	0.071	0.217	0.163	0.047	0.103	0.299	0.231	0.066
	500	1.0	0.089	0.103	0.098	0.005	0.059	0.073	0.066	0.004	0.089	0.103	0.098	0.005
		2.0	0.089	0.108	0.099	0.006	0.060	0.076	0.067	0.005	0.089	0.108	0.099	0.006
		5.0	0.091	0.180	0.106	0.016	0.060	0.122	0.073	0.012	0.091	0.180	0.106	0.016
		10.0	0.091	0.126	0.106	0.008	0.058	0.102	0.070	0.009	0.091	0.126	0.106	0.008
		20.0	0.092	0.254	0.125	0.039	0.060	0.175	0.084	0.029	0.092	0.254	0.125	0.039
0.5, 0.5	100	1.0	0.063	0.081	0.068	0.004	0.043	0.077	0.055	0.009	0.102	0.112	0.107	0.002
		2.0	0.062	0.135	0.071	0.013	0.043	0.121	0.061	0.016	0.092	0.198	0.109	0.018
		5.0	0.065	0.192	0.084	0.030	0.045	0.185	0.075	0.031	0.095	0.265	0.124	0.040
		10.0	0.063	0.216	0.111	0.049	0.044	0.211	0.103	0.049	0.097	0.298	0.159	0.066
		20.0	0.075	0.215	0.170	0.044	0.070	0.208	0.164	0.044	0.107	0.299	0.238	0.061
	500	1.0	0.061	0.068	0.063	0.002	0.042	0.059	0.046	0.005	0.104	0.111	0.108	0.002
		2.0	0.062	0.071	0.064	0.002	0.043	0.064	0.049	0.008	0.091	0.111	0.105	0.007
		5.0	0.062	0.086	0.069	0.006	0.043	0.085	0.059	0.011	0.091	0.122	0.106	0.007
		10.0	0.062	0.077	0.069	0.004	0.044	0.077	0.059	0.010	0.096	0.118	0.105	0.004
		20.0	0.062	0.163	0.074	0.020	0.043	0.157	0.064	0.022	0.093	0.227	0.114	0.026

Table A.16
Case study 3, pose 2: superimposition results for the CMA-ES algorithm.

β_1, β_2	Evaluations	θ	Fitness				MSE				MAX			
			m	M	μ	σ	m	M	μ	σ	m	M	μ	σ
1, 0	55,200	0.00001	0.036	0.105	0.056	0.024	0.036	0.105	0.056	0.024	0.121	0.242	0.158	0.028
		0.00010	0.036	0.110	0.059	0.026	0.036	0.110	0.059	0.026	0.111	0.286	0.153	0.033
		0.00100	0.036	0.109	0.061	0.028	0.036	0.109	0.061	0.028	0.127	0.220	0.159	0.023
		0.01000	0.036	0.118	0.055	0.026	0.036	0.118	0.055	0.026	0.113	0.234	0.153	0.029
		0.10000	0.036	0.134	0.068	0.032	0.036	0.134	0.068	0.032	0.138	0.262	0.172	0.038
		0.30000	0.036	0.676	0.163	0.167	0.036	0.676	0.163	0.167	0.128	0.929	0.296	0.224
	276,000	0.00001	0.036	0.061	0.037	0.005	0.036	0.061	0.037	0.005	0.144	0.169	0.146	0.005
		0.00010	0.036	0.061	0.037	0.005	0.036	0.061	0.037	0.005	0.143	0.172	0.146	0.005
		0.00100	0.036	0.062	0.038	0.007	0.036	0.062	0.038	0.007	0.144	0.181	0.147	0.008
		0.01000	0.036	0.061	0.037	0.005	0.036	0.061	0.037	0.005	0.144	0.174	0.146	0.005
		0.10000	0.036	0.036	0.036	0.000	0.036	0.036	0.036	0.000	0.144	0.145	0.145	0.000
		0.30000	0.036	0.124	0.053	0.029	0.036	0.124	0.053	0.029	0.111	0.297	0.158	0.042
0, 1	55,200	0.00001	0.089	0.809	0.136	0.129	0.063	0.559	0.092	0.090	0.089	0.809	0.136	0.129
		0.00010	0.090	0.177	0.119	0.028	0.062	0.116	0.078	0.015	0.090	0.177	0.119	0.028
		0.00100	0.090	0.166	0.120	0.022	0.063	0.106	0.078	0.013	0.090	0.166	0.120	0.022
		0.01000	0.089	0.174	0.117	0.026	0.061	0.099	0.074	0.012	0.089	0.174	0.117	0.026
		0.10000	0.089	0.176	0.119	0.026	0.063	0.103	0.077	0.013	0.089	0.176	0.119	0.026
		0.30000	0.090	0.929	0.249	0.226	0.063	0.676	0.163	0.152	0.090	0.929	0.249	0.226
	276,000	0.00001	0.090	0.108	0.098	0.006	0.060	0.073	0.066	0.004	0.090	0.108	0.098	0.006
		0.00010	0.089	0.108	0.098	0.007	0.063	0.073	0.067	0.004	0.089	0.108	0.098	0.007
		0.00100	0.089	0.108	0.098	0.007	0.063	0.074	0.067	0.004	0.089	0.108	0.098	0.007
		0.01000	0.089	0.108	0.100	0.006	0.063	0.075	0.067	0.005	0.089	0.108	0.100	0.006
		0.10000	0.089	0.101	0.092	0.004	0.063	0.071	0.068	0.002	0.089	0.101	0.092	0.004
		0.30000	0.090	0.129	0.096	0.009	0.063	0.089	0.067	0.005	0.090	0.129	0.096	0.009
0.5, 0.5	55,200	0.00001	0.062	0.116	0.078	0.018	0.042	0.107	0.064	0.019	0.092	0.184	0.123	0.026
		0.00010	0.062	0.123	0.084	0.022	0.042	0.118	0.069	0.025	0.092	0.184	0.130	0.028
		0.00100	0.062	0.132	0.080	0.019	0.044	0.117	0.066	0.021	0.092	0.197	0.127	0.025
		0.10000	0.062	0.135	0.074	0.018	0.044	0.131	0.061	0.020	0.092	0.185	0.117	0.022
		0.30000	0.062	0.687	0.168	0.176	0.042	0.676	0.150	0.171	0.092	0.929	0.247	0.242
		0.00001	0.062	0.077	0.063	0.003	0.044	0.071	0.048	0.007	0.091	0.110	0.105	0.004
	276,000	0.00010	0.062	0.067	0.063	0.002	0.044	0.061	0.047	0.006	0.092	0.110	0.105	0.005
		0.00100	0.062	0.077	0.065	0.005	0.044	0.072	0.051	0.010	0.092	0.109	0.106	0.004
		0.01000	0.062	0.067	0.063	0.002	0.044	0.061	0.046	0.005	0.092	0.107	0.106	0.003
		0.10000	0.062	0.067	0.062	0.001	0.044	0.055	0.044	0.002	0.105	0.107	0.106	0.000
		0.30000	0.062	0.123	0.069	0.016	0.043	0.121	0.054	0.019	0.091	0.180	0.112	0.020
		0.00001	0.062	0.067	0.064	0.002	0.044	0.062	0.051	0.008	0.091	0.107	0.102	0.007

References

[1] Annual HUMIE awards for human-competitive results produced by genetic and evolutionary computation. <www.human-competitive.org> (visited 9.10.08).
[2] S. Al-Amad, M. McCullough, J. Graham, J. Clement, A. Hill, Craniofacial identification by computer-mediated superimposition, Journal of Forensic Odontostomal 24 (2006) 47–52.
[3] A. Arcuri, X. Yao, Search based software testing of object-oriented containers, Information Sciences 178 (15) (2008) 3075–3095.
[4] M.Y. Aulsebrook, W.A. Iscan, J.H. Slabbert, P. Becker, Superimposition and reconstruction in forensic facial identification: a survey, Forensic Science International 75 (2–3) (1995) 101–120.
[5] T. Bäck, Evolutionary Algorithms in Theory and Practice: Evolution Strategies, Evolutionary Programming, Genetic Algorithms, Oxford University Press, 1996.
[6] T. Bäck, D.B. Fogel, Z. Michalewicz (Eds.), Handbook of Evolutionary Computation, IOP Publishing Ltd., Oxford University Press, 1997.
[7] L. Ballerini, O. Cordón, S. Damas, J. Santamaría, I. Alemán, M. Botella, Craniofacial superimposition in forensic identification using genetic algorithms, in: Proceedings of the IEEE International Workshop on Computational Forensics, Manchester, UK, 2007, pp. 429–434.
[8] L. Ballerini, O. Cordón, S. Damas, J. Santamaría, I. Alemán, M. Botella, Craniofacial superimposition in forensic identification using genetic algorithms, Tech. Rep. AFE 2008-03, European Centre for Soft Computing 2008.
[9] P.J. Besl, N.D. McKay, Iterative point matching for registration of free-form curves and surfaces, IEEE Transactions on Pattern Analysis and Machine Intelligence 14 (1992) 239–256.
[10] Y. Bilge, P. Kedici, Y. Alakoc, K. Ulkuer, Y. Ilkyaz, The identification of a dismembered human body: a multidisciplinary approach, Forensic Science International 137 (2003) 141–146.
[11] T. Blickle, Tournament selection, in: T. Bäck, D.B. Fogel, Z. Michalewicz (Eds.), Handbook of Evolutionary Computation, IOP Publishing Ltd., Oxford University Press, 1997. C2.3:1–C2.3:4.
[12] K.W. Bowyer, K. Chang, P. Flynn, A survey of approaches and challenges in 3D and multi-modal 3D + 2D face recognition, Computer Vision and Image Understanding 101 (2006) 1–15.
[13] M.J. Clarkson, D. Rueckert, D.L.G. Hill, D.J. Hawkes, Using photo-consistency to register 2D optical images of the human face to a 3D surface model, IEEE Transactions on Pattern Analysis and Machine Intelligence 23 (11) (2001) 1266–1280.
[14] O. Cordón, S. Damas, J. Santamaría, A fast and accurate approach for 3D image Registration using the scatter search evolutionary algorithm, Pattern Recognition Letters 27 (11) (2006) 1191–1200.
[15] O. Cordón, S. Damas, J. Santamaría, Feature-based image registration by means of the CHC evolutionary algorithm, Image and Vision Computing 24 (5) (2006) 525–533.

[16] O. Cordón, S. Damas, J. Santamaría, A practical review on the applicability of different EAs to 3D feature-based registration, in: S. Cagnoni, E. Lutton, G. Olague (Eds.), Genetic and Evolutionary Computation in Image Processing and Computer Vision, EURASIP Book Series on SP&C, 2007, pp. 241–263.
[17] K. Deb, R.B. Agrawal, Simulated binary crossover for continuous search space, Complex Systems 9 (1995) 115–148.
[18] H. Dong, J. He, H. Huang, W. Hou, Evolutionary programming using a mixed mutation strategy, Information Sciences 177 (1) (2007) 312–327.
[19] A. Eiben, J. Smith, Introduction to Evolutionary Computing, Springer-Verlag, 2003.
[20] L.J. Eshelman, Real-coded genetic algorithms and interval schemata, in: L.D. Whitley (Ed.), Foundations of Genetic Algorithms, vol. 2, Morgan Kaufmann, San Mateo, 1993, pp. 187–202.
[21] J.D. Foley, Computer Graphics: Principles and Practice, Addison-Wesley, 1995.
[22] A. Ghosh, P. Sinha, An economised craniofacial identification system, Forensic Science International 117 (1-2) (2001) 109–119.
[23] D.E. Goldberg, Genetic Algorithms in Search, Optimization, and Machine Learning, Addison-Wesley, Reading, MA, 1989.
[24] M.I. Goos, I.B. Alberink, A.C. Ruifrok, 2D/3D image (facial) comparison using camera matching, Forensic Science International 163 (2006) 10–17.
[25] N. Hansen, Compilation of results on the CEC benchmark function set, Tech. Rep., Institute of Computational Science, ETH Zurich, Switzerland, 2005. Available as <http://www.ntu.edu.sg/home/epnsugan/index_files/CEC-05/compareresults.pdf>.
[26] N. Hansen, A. Ostermeier, Completely derandomized self-adaptation in evolution strategies, Evolutionary Computation 9 (2) (2001) 159–195.
[27] N. Hansen, A. Ostermeier, Adapting arbitrary normal mutation distributions in evolution strategies: the covariance matrix adaptation, in: Proceedings of the 1996 IEEE International Conference on Evolutionary Computation, Piscataway, New Jersey, 312–317.
[28] F. Herrera, M. Lozano, J.L. Verdegay, Tackling real-coded genetic algorithms: operators and tools for the behavioural analysis, Artificial Intelligence Reviews 12 (4) (1998) 265–319.
[29] O. Ibáñez, O. Cordón, S. Damas, J. Santamaría, Craniofacial superimposition based on genetic algorithms and fuzzy location of cephalometric landmarks, in: Hybrid Artificial Intelligence Systems, LNAI, vol. 5271, 2008, pp. 599–607.
[30] M.Y. Iscan, Introduction to techniques for photographic comparison, in: M.Y. Iscan, R. Helmer (Eds.), Forensic Analysis of the Skull, Wiley, 1993, pp. 57–90.
[31] R. Koza, M.J. Streeter, M.A. Keane, Routine high-return human-competitive automated problem-solving by means of genetic programming, Information Sciences 178 (23) (2008) 4434–4452.
[32] W.M. Krogman, M.Y. Iscan, The Human Skeleton in Forensic Medicine, second ed., Charles C. Thomas, Springfield, IL, 1986.
[33] Z. Michalewicz, Genetic Algorithms + Data Structures = Evolution Programs, Springer-Verlag, 1996.
[34] B.A. Nickerson, P.A. Fitzhorn, S.K. Koch, M. Charney, A methodology for near-optimal computational superimposition of two-dimensional digital facial photographs and three-dimensional cranial surface meshes, Journal of Forensic Sciences 36 (2) (1991) 480–500.
[35] T. Nomura, K. Shimohara, An analysis of two-parent recombinations for real-valued chromosomes in an infinite population, Evolutionary Computation 9 (3) (2001) 283–308.
[36] A. Ricci, G.L. Marella, M.A. Apostol, A new experimental approach to computer-aided face/skull identification in forensic anthropology, Am. J. Forensic Med. Pathol. 27 (1) (2006) 46–49.
[37] A.H. Ross, Use of digital imaging in the identification of fragmentary human skeletal remains: a case from the Republic of Panama, Forensic Science Communications 6 (4) (2004).
[38] J.M. Rouet, J.J. Jacq, C. Roux, Genetic algorithms for a robust 3-D MR-CT registration, IEEE Transactions on Information Technology in Biomedicine 4 (2) (2000) 126–136.
[39] J. Santamaría, O. Cordón, S. Damas, Evolutionary approaches for automatic 3D modeling of skulls in forensic identification, in: Applications of Evolutionary Computing, LNCS, vol. 4448, 2007, pp. 415–422.
[40] J. Santamaría, O. Cordón, S. Damas, I. Alemán, M. Botella, A scatter search-based technique for pair-wise 3D range image registration in forensic anthropology, Soft Computing 11 (9) (2007) 819–828.
[41] J. Santamaría, O. Cordón, S. Damas, J.M. García-Torres, A. Quirin, Performance evaluation of memetic approaches in 3D reconstruction of forensic objects, Soft Computing (2009), doi:10.1007/s00500-008-0351-7.
[42] F.Y. Shih, C. Chuang, Automatic extraction of head and face boundaries and facial features, Information Sciences 158 (2004) 117–130.
[43] L. Silva, O. Bellon, K. Boyer, Robust Range Image Registration Using Genetic Algorithms and the Surface Interpenetration Measure, World Scientific, 2005.
[44] P. Sinha, A symmetry perceiving adaptive neural network and facial image recognition, Forensic Science International 98 (1-2) (1998) 67–89.
[45] P. Suganthan, N. Hansen, J. Liang, K. Deb, Y. Chen, A. Auger, S. Tiwari, Problem definitions and evaluation criteria for the CEC 2005 special session on real parameter optimization, Tech. rep., Nanyang Technological University, 2005. Available as <http://www.ntu.edu.sg/home/epnsugan/index_files/CEC-05/Tech-Report-May-30-05.pdf>.
[46] D.H. Ubelaker, A history of Smithsonian-FBI collaboration in forensic anthropology, especially in regard to facial imagery, Forensic Science Communications 2 (4) (2000).
[47] D.H. Ubelaker, E. Bubniak, G. O'Donnel, Computer-assisted photographic superimposition, Journal of Forensic Sciences 37 (3) (1992) 750–762.
[48] A. Ugur, Path planning on a cuboid using genetic algorithms, Information Sciences 178 (16) (2008) 3275–3287.
[49] H. Welcker, Der schädel Dantes (in German), in: K. Witte, G. Boehmer (Eds.), Jahrbuch der deutschen Dantegesellschaft, vol. 1, Brockhaus, Liepzig, 1867, pp. 35–56.
[50] S.M. Yamany, M.N. Ahmed, A.A. Farag, A new genetic-based technique for matching 3D curves and surfaces, Pattern Recognition 32 (1999) 1817–1820.
[51] M. Yoshino, H. Matsuda, S. Kubota, K. Imaizumi, S. Miyasaka, S. Seta, Computer-assisted skull identification system using video superimposition, Forensic Science International 90 (1997) 231–244.
[52] Z. Zhang, Iterative point matching for registration of free-form curves and surfaces, International Journal of Computer Vision 13 (2) (1994) 119–152.
[53] Z. Zheng, J. Jiong, D. Chunjiang, X. Liu, J. Yang, Facial feature localization based on an improved active shape model, Information Sciences 178 (9) (2008) 2215–2223.
[54] B. Zitova, J. Flusser, Image registration methods: a survey, Image and Vision Computing 21 (2003) 977–1000.